INSTITUTE OF TECHNOLOGY

AIR UNIVERSITY

UNITED STATES AIR FORCE

SCHOOL OF ENGINEERING

THESIS

NOX

WRIGHT-PATTERSON AIR FORCE BASE, OHIO

AF-WP-B-SEP 60 5M

A STUDY OF SHOCK WAVES

MOVING OVER A TRANSVERSELY SLOTTED WALL

THESIS

Presented to the Faculty of the School of Engineering of

the Institute of Technology

Air University

in Partial Fulfillment of the

Requirements for the Degree of

Master of Science

By

Oscar Mauterer, B.S. M. E.

Captain USAF

Graduate Astronautics

August 1961

Preface

The requirement for this study of shock wave interaction with slotted walls was the result of a previous investigation on a shock tube with perforated walls. The slotted walls were chosen to simplify the flow phenomena in an attempt to better understand the shock interaction with the disturbance to flow.

I would like to acknowledge my indebtedness to Doctor Andrew Shine, my faculty advisor, whose guidance and aid during this study were cheerfully and willingly given.

Mr. John Parks, my laboratory assistant, gave me outstanding support in solving numerous laboratory test problems

The numerous machining operations required for this study could not have been accomplished without the full cooperation of Mr. M. W. Wolfe, supervisor of the Institute of Technology School Shops.

I am deeply indebted to Mr. Thomas Long, Tektronic Inc. Field Engineer, whose technical assistance in the electronic instrumentation of this study was invaluable.

I wish to acknowledge my special indebtedness to my wife for her patience and understanding throughout this undertaking and for typing the numerous tables found in this report .

Contents

List of Figures

List of Tables

List of Symbols

A	Cross sectional area of shock tube
C	Velocity of sound, ft./sec.
k	specific heat ratio
$\dot{m}$	Mass rate of flow
M_s	Mach number of the shock wave
p	pressure, psi
P	Pressure ratio
T	Temperature, degrees Rankine
u	Velocity, ft./sec.
W_s	Velocity of the shock wave relative to the shock tube, ft./sec.
Z	Percent attenuation, %.
Δ	Change
ρ	Density

Subscripts

1. Low pressure region in front of shock wave
2. Region between shock wave and contact surface
3. Region between contact surface and expansion wave
4. High pressure region before diaphragm rupture

21 A ratio, i.e. $P_{21} = \frac{p_2}{p_1}$

s Shock wave condition

Abstract

This experimental study investigated the effect on a shock wave as it passes a pair of transversely slotted test plates which were in the top and bottom walls of a rectangular shock tube. The shock strength, defined as the pressure ratio across the shock for this study, was of primary interest. The shock wave response to the disturbance was verified by Schlieren photography. The slot width, the slot entrance radius, the effective slot depth, and the strength of the incident shock wave were varied to determine the effects of these parameters. The attenuation was found from pressure measuring transducer data which was recorded photographically. The time to establish the quasi-steady flow of air out through the openings determined the extent of attenuation. When the slot width or slot entrance radius were large, the reflected shock waves generated at the disturbance were sufficiently strong to delay the mass flow out of the opening; thus, the attenuation was reduced. The attenuation increased as the effective slot depth was decreased. Schlieren photography verified the formation of the reflected shock waves and the formation of the rarefaction waves associated with the loss of mass behind the shock wave.

A STUDY OF SHOCK WAVES MOVING OVER A TRANSVERSELY SLOTTED WALL

I. Introduction

Purpose

The purpose of this study is to determine by experiment what effect transverse slots in the walls of a shock tube have on the strength of the incident shock wave. The strength of the shock wave for this study is the ratio of pressure behind the moving shock wave to the pressure ahead of the shock wave. The transverse slots were placed normal to the flow in test plates with surfaces which were flush with the upper and lower inside walls of the shock tube.

Background Information

Cameron (Ref 1) conducted an experimental study of shock waves moving over a perforated wall with and without flow through the holes prior to shock wave arrival. The requirement for that study was established when the results of experiments (Ref 5), conducted to determine the effect of a moving shock wave on flame fronts in combustion chambers that required an exhaust system, were considered inconclusive. The exhaust system of the combustion experiment necessitated perforations in the walls of the shock tube. Since the properties of the shock wave after passing over the perforations

were not known and had to be assumed, the combustion experiment results were questionable.

Since Cameron's study entailed a complex interaction of flow phenomena which precluded extensive quantitative results, the requirement for this study was established to further the understanding of the flow phenomena.

Scope of Study

Several configurations were used to determine the effect on the incident shock wave. The total open area was varied for different radii of the slot opening on the inside wall of the test plates. The effective depth of the slot was also varied. In addition, the effects of perforations were studied and compared to a slot with comparable open area.

The following chapters contain a preliminary discussion of the phenomena, a description of the apparatus and test procedures, an evaluation of the test results, and a summary of results and recommendations. The appendix has sample calculations, photographic results, tables and graphs of the data, drawings, and an error analysis of data scatter.

II. Preliminary Discussion

One-Dimensional Analysis of Shock Tube

Numerous theoretical analysis (Ref 6:5-108;9:922-1027 and others) have developed basic shock tube relations which have been experimentally verified for normal shock tubes (Ref 3:14). The basic considerations are summarized to establish the terms and relationships for this study.

The model of the basic shock tube, Fig.1, is a long, constant cross-sectional area tube which has a diaphragm that separates the high pressure region, 4, and the low pressure region, 1, of the tube. The temperatures of both regions, T_1 and T_4, are assumed equal. When the diaphragm is ruptured, expansion waves propagate into region 4 with the later waves travelling at progressively lower speeds because the temperature is lowered as each wave progresses to the end of the tube. However, the compression waves travelling in region 1 coalesce to form a shock front as the later waves move at progressively higher speeds. Since there is no entropy change across the expansions waves but there is an entropy change across a shock wave, a contact surface or temperature discontinuity separates the gas in the region between the expansion waves and the shock front. The high and low temperature regions, separated by the contact surface, are designated regions 2 and 3 and have the same pressure and velocity. The pressure and flow velocity for regions 2 and 3 are p_2 and u_2, p_3 and u_3, respectively.

The shock front velocity relative to the shock tube is W_s. Since the flow velocity, u_1, in region 1 is zero the shock speed is also

relative to region 1, and the Mach number is equal to the shock velocity divided by the speed of sound in region 1, C_1.

Shock Wave Strength

Hall (Ref 7:238) presents a theoretical analysis, assuming one-dimensional unsteady flow, and defines shock strength as the ratio of pressure, temperature, or density of the gas immediately behind the moving shock wave to that ahead of it. The ratio of pressures, P_{21}, is used for this study to measure the shock strength.

The expression for the shock wave pressure ratio is

$$P_{21} = 1 + \frac{2K}{K+1}\left[\left(\frac{W_s}{C_1}\right)^2 - 1\right] \tag{1}$$

where k is the specific heat ratio. For air with k approximately equal to 1.4, equation (1) reduces to

$$P_{21} = \frac{7\left(\frac{W_s}{C_1}\right)^2 - 1}{6} \tag{2}$$

Attenuation Computation Method

Huber and McFarland (Ref 8:20-22) outline a method for calculating the attenuation of a shock wave which has been adapted for this study. The difference between the shock strength before and after passing the disturbance is the shock strength loss, $\frac{\Delta P_2}{P_1}$.

The shock-pressure attenuation, z, is

$$z = \frac{\frac{\Delta p_2}{p_1}}{\frac{p_2}{p_1} - 1} \tag{3}$$

Z, the per cent attentuation, is found when equation (3) is multiplied by 100. Appendix B shows the per cent attentuation equation further altered to more readily use the experimentally obtained data.

A positive value of Z indicates a decrease in the shock strength; negative value indicates an increase in shock wave strength.

Attentuation of a Shock Wave in a Tube

An analysis (Ref 3:4-8) of the interrelation of the mass flows associated with shock movement is summarized here.

When the diaphragm is burst, in the absence of viscosity, the entire mass of air in the region between the expansion wave and shock wave is placed in motion with velocity u_2. This initial mass rate of flow, $\dot{m}_1$, for a given shock tube cross-sectional area, A, is

$$\dot{m}_1 = \rho_2 u_2 A \tag{4}$$

Since the mass flow in the region behind the shock may decrease because of boundary layer action or other disturbances, the mass flow, $\dot{m}$, may also be a function of the time and distance after passing the disturbance.

Now, the shock wave also places into motion a mass flow, $\dot{m}_s$, which

is determined by the following equation:

$$\dot{m}_s = \rho_1 C_1 A \frac{5}{\sqrt{17}} \sqrt{6P_{21}+1}\ \frac{P_{21}-1}{P_{21}+6} \qquad (5)$$

When $\dot{m}_s$ is greater than $\dot{m}$, expansion waves are generated which will catch up with the shock front and reduce the shock strength. Both compression and expansion waves generated behind the shock wave will travel at the local speed of sound relative to the fluid in which they travel. Since the fluid velocity relative to the shock tube plus the local speed of sound behind a shock is greater than the shock wave velocity, all waves formed behind the shock front will overtake it. If $\dot{m}_s$ is less than $\dot{m}$, the generated compression waves will strengthen the shock front when it is overtaken. If there is no disturbance to the flow in the region behind the shock wave, then $\dot{m}_s$ equals $\dot{m}$ and neither expansion nor compression waves are generated behind the shock wave.

Attentuation Effects of a Slotted Wall. Eckhaus (Ref 4:10) described the mechanism of oblique shock reflection on a wall with transverse slots. The applicable portion of the analysis for a shock tube with a normal shock front is illustrated in Figure 2. Since the pressure behind the shock wave is greater than the atmospheric pressure, an expansion flow originates at the beginning of the slot, point A. The flow at the slot will have a velocity component perpendicular to the wall from the action of the expansion fan. After passing the far side of the slot, point B, the flow must once again be tangential to the wall; therefore, a compression wave originates at point B since the flow is turned toward the wave.

When the flow out of the wall opening has been established, the loss of mass flow in the region behind the shock wave will cause $\dot{m}$ to be less than $\dot{m}_s$ which will generate expansion waves. These expansion waves, F in Figure 22, weaken the shock when they overtake it, D to E in Figure 22.

In a study of the pressure response of a transducer placed at the end of a gauge line, which was perpendicular to the flow direction in a shock tube, Crichton (Ref 2:23,24,27) showed that a shock wave was generated in the gauge line. The induced shock wave travelled up into the line and was weaker than the primary incident wave. The generation of the shock wave in the gauge line was compared to the bursting of a diaphragm at the mouth of the line; therefore, one-dimensional analysis of the wave interaction in the gauge line was used. If a shock wave were induced in the slotted wall the unsteady flow expansion waves, associated with the induced shock wave, would also weaken the incident wave. The induced shock wave would also reflect from the open boundary as an expansion wave.

Shock Transit Over Slot. The shape of a shock wave during formation after diaphragm rupture was investigated by NACA (Ref 8:20). Initially, the shock wave was not one-dimensional nor normal to the flow, but it became normal to the flow as it progressed downstream.

Cameron's analysis (Ref 1:11) on the effect of perforations on the orientation of a shock wave is applicable for this study. Since the

thickness of a shock wave is many orders of magnitude less than the dimensions of the slot, it may be possible to relate the slot to two sharp-cornered discontinuities even though the slot is flush with the inside surface of the shock tube. Sun (Ref 11:12) predicted the strengthening of the disturbed portion of the incident wave by reflected shock waves from a right-angled edge. However, the face of the shock wave did not remain normal to the flow in order to satisfy the normal and tangential boundary conditions. Since the shock wave becomes normal to the flow after diaphragm burst, in a similar manner the shock wave should become normal to the flow direction farther downstream from the sharp-cornered discontinuity.

Summary of Possible Effects. The phenomena which can occur when a shock front passes over an open wall is indeed complex. The time sequence of events could produce a stronger or weaker incident shock wave with a change in orientation to the shock tube. As the shock wave crosses the opening, the portion of the wave in contact with the disturbance will initially be weakened and slowed up. After passing the opening the shock wave could be strengthened by the reflected shock and compression waves originating at the far edge. When the flow out the opening is established, the primary incident shock wave strength would be decreased by the expansion waves generated by the loss of mass flow rate behind the shock.

III. Description of Apparatus

The shock tube and associated equipment of the Institute of Techology's Mechanical Engineering Laboratory were used for the test runs. Figure 3 is a schematic drawing of the test equipment and Figure 4 shows a general view of the shock tube. The shock tube and test equipment are described in the following sections.

Shock Tube

The Institute of Technology's shock tube is twenty feet long and has an inside rectangular cross section, four inches wide by eight inches high. It consists of five four-foot long sections with the first section used as a high-pressure chamber. Mylar film is used as the diaphragm material between sections 1 and 2 which are clamped together by two 2000 psi hydraulic actuating cylinders. Section 5, which has a pair of six-inch diameter viewing ports, was disengaged from section 4 and moved downstream to allow an 18-inch long test section to be placed between them. The 18-inch long test section, Fig. 5, was designed for a study of shock waves moving over a perforated wall (Ref 1:15).

Section 4 has three locations in which Endevco Model 2501-500 pressure transducers may be mounted flush with the inside of the shock tube. These stations are located 100 in., 128 in. and 140 in. downstream from the diaphragm and are designated stations A, B, and C respectively for this study.

Section 5 has two transducer receptacles that are 3 7/8 in. and 28 in. from the upstream end of section 5. These positions are

designated stations D and E, respectively.

Air was used for both driver and driven gases for all runs. The driver gas was dry, oil-free air from the laboratory's compressed air system. The low pressure section contained the driven air at room temperature and pressure since the test plates with slots or perforations precluded evacuation of this section.

Test Section

The test section, Fig. 5, has inside dimensions which are equal to that of the shock tube's inside cross section. It was designed to mate flush with sections 4 and 5 to preclude disturbing the flow. The vertical side plates were extended above the shock tube to mount two six-inch diameter, optically flat glass view-ports, whose centers coincided with the top inside wall of the test section. This design allowed the maximum field of view at the top wall for Schieren photography of the interaction of the shock wave with the disturbance.

Two openings, which measured 6 in. by 4 in. in the outside and 4 in. by 4 in. in the inside of the top and bottom walls, were used to hold the different pairs of test plates, Fig. 5 . Six threaded holes in the top and bottom were used to hold the test plates securely in position. The test section and test plates were fabricated from one-inch thick aluminum jig plate.

Test Plates

Twenty-eight different configurations of test plates were fabricated for this study. The holes and slots were machined into the

4 in. by 4 in. face of different pairs of plates. These plates were milled for a forced fit into the openings in the test section. Special care was taken to insure that the inside surface of the test plate was flush with the inside of the test section to preclude any disturbance to the flow. Figures 6, 7 and 8 are representative pictures of the test plates. The following is a list of the total open area of each test plate used in the study.

A. Blank plates

B. 0.130 in. slot: open area = 0.480 $in.^2$

C. 0.500 in. diameter holes: open area = 0.982 $in.^2$

D. 0.281 in. slot: open area = 1.036 $in.^2$

E. 0.400 in. slot: open area = 1.469 $in.^2$

F. 0.508 in. slot: open area = 1.844 $in.^2$

G. 0.750 in. slot: open area = 2.704 $in.^2$

The holes and slots were initially machined straight through the test plates which presented sharp openings to the flow. The slots were machined to within 1/8 in. of each edge of the plates so that the major portion of the shock wave would be affected. The plates with holes, shown in Fig. 6, used by Cameron (Ref 1:17) in his study of flow over perforations, were drilled so that the major portion of the shock wave would also be affected. The opening of the slots and holes, which were on the inside surface of the shock tube wall, were machined with different radii as listed in Table I. All radii were cut to full depth.

Table I. Entrance Radius Versus Slot Width of Test Plate

Radius Inch	Slot Width- Inch					0.500" Dia. Hole
	0.130	0.281	0.400	0.508	0.750	
0	X	X	X	X	X	X
1/16	X	X	X	X	X	
1/8	X	X	X	X	X	X
1/4		X	X	X	X	X
3/8		X	X	X	X	

Note: (X) Indicates the test plate configuration was tested.

The 0.130 in. wide slot test plates were countermilled slightly to a depth of 0.475 in. from the top; whereas, all other configurations were initially milled out uniformly for the full depth of the plates.

The 0.400 in. wide slot with 3/8 in. radius of entrance plates were also countermilled 1.500 in. wide to a depth of 0.250 in. and 0.500 in. from the top surface for two additional configurations. Since the plate thickness was initially 0.980 in., the effective slot depth was 0.730 in. and 0.480 in. for the above countermilled test plates.

Slot Extensions

A pair of test plate slot extensions, Fig. 9, were fabricated of 0.035 in. thick brass sheet to fit on the 0.400 in. slot test plates of full thickness. The extensions were 4 inches long which gave an effective slot length of 5 inches for this configuration. The opening of the extension was flush with the slot opening in the test plate.

Slot Cover Plates

A pair of 1/8 inch thick cover plates, Fig. 9, were used to fit over the 0.400 in. slot test plates. The plates were also used for the countermilled test plate runs.

Manometers

The high pressure readings in region 4 were obtained with a 150 inch mercury manometer and the low pressure readings downstream, region 1, were obtained from barometric pressure readings on a 35 in. glass tube mercurial barometer.

Transducers

The pressure step across the shock wave was measured with Endevco Corporation Model 2501-500 piezoelectric transducers. These transducers have a linear voltage response to the induced pressure step and are designed to operate in a temperature range of (-)30 to (+)80 degrees C. up to rated values of 30 volts at 500 psi.

Electronic Instrumentation

Two oscilloscopes, Fig. 10, were used for this study: a Tektronic Type 531 and Hickok Type 1805.

Type 531 Oscilloscope. A Tektronic Type 531 oscilloscope, with a Tektronic 53/54D vertical deflection plug-in preamplifier and a Tektronic 123 trigger preamplifier, was used to obtain a voltage-time plot from two transducers. The vertical deflection system, with a

calibrated range from 1 millivolt/cm to 50 volt/cm, permits two different transducer outputs to be recorded on the oscilloscope trace with a two percent accuracy. The oscilloscope's horizontal sweep speed rate of 0.02 microseconds per cm. to 12 sec. per cm. has a three percent accuracy. The Type 123 trigger preamplifier increases 100 times the trigger input from a transducer to initiate the oscilloscope's sweep. This oscilloscope has been modified to include a single sweep circuit which prevents retriggering of the horizontal sweep after the initial passage of the shock wave over the triggering transducer.

Type 1805 Oscilloscope. A Hickok Type 1805 oscilloscope with a Tektronic Type 53-B vertical deflection plug-in preamplifier was used to obtain a voltage time plot from one transducer and to trigger the light source for the Schlieren system. This oscilloscope has a sweep delay circuit which allows a preselected time delay of the sweep after a trigger signal has been received. Delay times from 100 milliseconds to almost instant triggering are available from a calibrated variable selector. The horizontal sweep speed rate and accuracy are the same as those of the Tektronic Type 531 oscilloscope. With the 53-B plug-in unit, the 1805 oscilloscope has a vertical deflection voltage range of 0.05 to 20 volts/cm for DC coupled operation with a rise time of approximately 0.017 microseconds.

Oscilloscope Cameras. Two Polaroid Land cameras, Fig. 11, were used to record the oscilloscopes' display. The mountings for the cameras were Fairchild Model F-296A and F-286 adapters for the Type 531

and 1805 oscilloscopes, respectively. Type 42 (ASA 200) film was used with lens opening of F 1.9.

Time Mark Generator. A Tektronic Type 181 Time Mark Generator, Fig. 11, was used for calibration of the horizontal sweep of both oscilloscopes. The time mark generator has an output range of 0.1 (sine wave) to 10,000 microseconds.

Schlieren System

Fig. 12 is a schematic drawing of the Schlieren optical system which was used for photographing the test section. The light source was a General Electric FT-230 spark lamp. The power supply for the spark lamp was assembled by technicians of the Mechanical Engineering Laboratory from a design presented in Ref 12. Prior calibration of the power supply indicated a useable spark duration of 5 microseconds with a one microsecond rise time. The time delay through the power supply to the spark lamp was 4 microseconds; therefore, the total time delay for the light source was 5 microseconds.

The photographs were taken with a Polaroid adapter back for a Graphlex camera mounted on a simple bellows, Fig. 13. No lens was used as the camera mount was positioned for proper focusing, and no shutter was required as the pictures were taken in a darkened room. Polaroid type 42 (ASA 200) film was used primarily but type 44 (ASA 400) also gave satisfactory results.

The parabolic mirrors in the Schlieren system were six inches in diameter and had a 30 inch focal length.

IV. Experimental Procedures

Two basic configurations were employed for this study. The first configuration was used for transducer calibration, and the second was used for the experimental runs.

Transducer Calibration Configuration

The electronic configuration used to calibrate the transducers is shown in Fig. 14. The test section was not placed between sections 4 and 5 of the basic shock tube when calibrating transducers 15, 18 and 16 which were at stations B, C and D, respectively. When the shock wave passed station A, transducer 17 generated a voltage which was amplified by the Type 123 preamplifier and triggered the sweep of the Type 531 oscilloscope. The initial straight portion of the trace, Fig. 16, is representative of p_1. Figure 18 is a sketch of the oscilloscope's presentation with the pressure steps at stations B and C noted. The horizontal distance from initiation of the trace, left edge of the oscilloscope picture in Fig. 16, to the transducer position as indicated by the pressure pulses of the downstream stations B and C represents the time to reach these stations.

The Type 1805 oscilloscope presentation was used to display the pressure step at station D. When the Type 531 oscilloscope was triggered from station A's transducer, a 25 volt square-wave gate signal with a rise time of 0.01 microsecond was initiated by the Type 531 to trigger the delaying sweep of the 1805. No delay of the sweep was used for this configuration. When the shock wave

passed Station D, transducer 16's response voltage was displayed on the Type 1805 delaying sweep. For a given run, it was therefore possible to obtain the shock-wave pressure steps at station B, C and D.

Experimental Runs Configuration

Fig. 15 is a schematic drawing of the electronic configuration used for the experimental runs. Transducer 17 at station B triggered the sweep on the Type 531 oscilloscope. As the shock wave passed transducers 15 and 16, stations C and D, the voltage response of these transducers was displayed by the Type 531's sweep, as shown in the sketch of Figure 18. Fig. 17 is a photograph of the oscilloscope's trace during an experimental run. The delaying sweep of the Type 1805 oscilloscope was used to display the pressure step at station E, transducer 18 location.

The main-sweep 150 volt sawtooth pulse, with a one microsecond rise time, of the 1805 scope was used to trigger the Schlieren system's light source. The triggering signal was delayed a predetermined time to photograph the test section phenomena during shock wave passage.

In this way, though the delaying sweep of the 1805 scope was also delayed by the predetermined time set to catch the shock wave in the test section, the values for the shock wave's pressure steps at station C, D and E could be recorded and Schlieren photography taken of the shock wave as it passed the disturbance to flow.

V. Evaluation of Data

The oscilloscope photographs were used for voltage versus time representations of the transducers' output. The photographs, Fig. 16 and 17, are read from left to right. The time for the shock to travel between stations is found by measuring the horizontal distance between the transducer response representations on the photograph. The response of the triggering transducer is the initiation of the sweep; whereas, the downstream transducers voltage output causes a vertical deflection of the oscilloscope trace. After transducer calibration the pressure steps, p_2-p_1, of the shock wave are found by measuring the vertical deflection of the sweep.

An error analysis to show the maximum probable fluctuation in data due to measurement inaccuracy is developed in Appendix C.

Transducer Calibration Results

The electronic configuration used to calibrate the transducers is shown in Figure 14. The average velocity of the shock wave between stations A and C was used with the speed of sound, based on the temperature in region 1, to determine the Mach number of the shock. The pressure ratio across the shock wave was then obtained from equation (2). With this pressure ratio and the pressure in region 1, the pressure step, p_2-p_1, was then found. The voltage deflections of the transducers versus the pressure steps, Table II, were then plotted and compared with the transducer calibration curves, Fig. 19,20,21, obtained by Cameron (Ref 1:69-71) for the same transducers. The scatter

of points from the curve is in good agreement with the scatter of points in the reference source. The curves were therefore used for the experimental runs.

Sample calculations for determining the plotted points is included in Appendix A.

Experimental Results

General. The electronic configuration used for the experimental runs is shown in Figure 15. From the voltage measurement on the oscilloscope photographs for each run the pressure steps at stations C, D, and E were obtained from the transducer calibration curves. The attenuation between stations C and D, Z_D, and the attenuation between stations C and E, Z_E, were determined from equation (4) as modified in the sample calculations in Appendix B. Since all the table values of attenuation for this study were positive which indicates a decrease in shock strength, the (+) sign has been omitted in the tables.

Attenuation Check of Test Section. To determine the attenuation inherent in the test configuration, twenty-four (24) individual runs were made with blank test plates in the test section. The results of these runs are found in Table III and IV which indicate average values of attenuation between stations C and D of 1.3% and between stations C and E of 7.2%. The value of attenuation between stations C and D is within the accuracy of the electronic instrumentation; therefore, this attenuation is assumed to be zero for subsequent comparison of test-plate configuration results.

Attenuation For 0.480 in.^{2} Open Area Per Plate. Thirty-six runs were made with a 0.130 in. wide slot milled through a pair of test plates. Three different radii of the entrance to the slot opening were used for this open area. The attenuation data for these runs are shown in Table V. Runs 63 through 74 were made periodically during the course of this study to check the proper functioning of the instrumentation. The results of these runs correlated with the previous runs for this configuration.

Attenuation For 1.036 in.^{2} Open Area Per Plate. Forty-nine runs were made with a 0.281 in. wide slot that had various entrance radii. The strength of the incident shock wave was varied and the attenuation for stations D and E was obtained for this open area when the entrance to the slot was sharp-edged (zero radius) and had a 1/8 in. radius. Table VI contains the results of these runs.

Attenuation For 1.469 in.^{2} Open Area Per Plate. The effective slot length was varied with slot extensions, Fig. 9, and by countermilling the test plates to different depths for the 0.400 in. wide slot, Fig. 8. Eighty-nine runs were made in which the effective depth of slot was varied from 0.480 inch to 5 inches while the slot entrance radius was varied from zero to 3/8 in.. The results of these runs are shown in Tables VII, VIII, IX and X. The attenuation vs. slot depth found in Table X is a summary of the data found in Tables VII, VIII, and IX for the 3/8 in. radius of the slot entrance.

Attenuation For 0.400 in. Wide Slot With Cover Plate Over Slot. Twenty-nine runs were made with the cover plates over the slotted test

plates. The effective depth of the test plates was varied by countermilling the test plates 1.500 inches wide to different depths. The radius of the entrance for all runs was 3/8 inch. The values for the attenuation are found in Table XI.

Attenuation For 1.844 in.^{2} Open Area Per Plate. The 0.508 in. wide slot was tested with all the radii of entrance available for this study. The attenuation at station D for the thirty-eight runs is shown in Table XII.

Attenuation For 2.704 in.^{2} Open Area Per Plate. Thirty-six runs were made with a 0.750 in. wide slot with the entrance radius varied from zero to 3/8 inch. The results for the attenuation at station D are shown in Table XIII.

Attenuation For 0.982 in.^{2} Open Area Per Plate. Twenty-one runs were made with five -0.500 in. diameter holes drilled through the test plates. The flow entrance radius was varied and the results for the attenuation are given in Table XIV.

Schlieren Photography. Schlieren photographs of the test-section flow phenomena were taken for all of the open areas. The shock wave is progressing from right to left in the representative pictures in Figures 22, 23, 24, 25, and 26. The double image to the left of the shock in Figures 22, 24, 25 and 26, and the thick appearance of the shock front in all the pictures was caused by the misalignment of the light through the test section. The effect of non-parallel light through the test section is analyzed and illustrated in Ref 10: 12, 18.

VI. Discussion of Results

Effect of P_{21} on Z_D

Figures 28 and 29 show the relation between the attenuation and pressure ratio across the shock wave for the 0.281 in. wide slot test plates with zero and 1/8 in. entrance radius. On inspection of the figures for the limited pressure ratio range from 1.475 to 2.412, there is no indication that the attenuation at stations C and D varied as a function of the pressure ratio. The range of pressure ratios studied was extremely limited; therefore, no conclusions can be made for stronger shock waves.

Effect of Time and Distance on Attenuation

From Tables V, VII, VIII, and XIV and Fig. 28 and 29, the difference in the average attenuations for stations D and E is much greater than the 7.2% obtained from the blank test plates during the attenuation check of the test section for station E. Since the values are for numerous test plate configurations, including five-0.500 in. diameter holes, it seems apparent that the attenuation is a function of the time and distance from the disturbance. The expansion waves, generated by the quasi-steady flow out of the wall openings behind the shock wave, will take a finite time, therefore distance, to overtake the shock.

Effect of Entrance Radius For Constant Open Area

0.130 Inch Slot. Table V values for station D average

attenuation show an approximately linear increase in attenuation as the entrance radius was increased to 1/8 inch. This trend indicated that a shorter time lag was required to establish the quasi-steady flow out of the larger radius opening; therefore, the generation of the rarefaction waves associated with the mass loss was expedited. Since only two radii were studied in addition to the straight through slot, no estimate can be made for larger radii of the slot entrance.

0.508 Inch and 0.750 Inch Slots. Figure 30 for these two slot openings shows a similar shape for the station D attenuation versus entrance radius curves. The attenuation initially decreases as the radius increases. After reaching minimum values of attenuation, the further increase in entrance radius was associated with an increased average value of attenuation at station D. The initial decrease in attenuation indicates that the reflected shock waves were delaying the establishment of the quasi-steady flow out of the openings. Since the 1/16 inch radius, small in size compared to the slot width, probably has little effect on the establishment of the flow out of the slot opening, the decrease in attenuation indicates that the reflected shock waves' strength is a function of time to cross the opening by the incident shock wave. For larger radii of entrance when the establishment of flow out would be easier, the effect of stronger reflected waves is diminished.

0.281 Inch Slot. Figure 30 shows the linear relation between the average value of station D attenuation and the entrance radius when the

entrance radius is 1/4 in. or less. This would indicate that the outward flow was established faster for the larger radii of entrance as in the case of the 0.130 in. wide slot. The attenuation at station D decreased for the 3/8 in. entrance radius of the slot opening. The decrease in attenuation indicates that the reflected shock waves, generated at the downstream edge of the slot opening, were delaying the establishment of the quasi-steady flow out of the openings; therefore, the generation of the rarefaction waves associated with the mass loss was delayed.

0.400 Inch Slot. Figure 31 indicates a nearly constant value of 15.3% for the attenuation at station D when the entrance radius is 1/8 inch or less. The attenuation decreased with a further increase in the entrance radius. For the condition of constant attenuation, stronger reflected cylindrical shock waves, generated at the downstream edge of the slot opening, apparently cancelled the effect of easier establishment of the flow out of the opening as the entrance radius increased. The decrease in attenuation at station D to the value of 7.7% for the 1/4 in. radius of the slot opening indicates that the cylindrical reflected waves were delaying the establishment of the quasi-steady flow out of the opening; hence, the generation of the expansion waves associated with the mass loss behind the incident shock wave was delayed.

Effect of Slot Depth on Attenuation

Table X demonstrates the rapid increase in attenuation as the effective slot depth was decreased below 0.980 in. for the 0.400 in.

slot with a 3/8 in. entrance radius. The cylindrical reflected shock waves, generated at the downstream edge of the slot opening, reflect from the open boundary as expansion waves. The decrease in slot depth decreases the time it takes to reflect the expansion waves; therefore, the establishment of the flow out of the opening is expedited.

Figure 31 is a comparison of the attenuation at station D for the 0.100 in. wide slot with various radii when the slot depth is 0.980 in. and 5 in.. The two curves have the same shape, and the difference in attenuation values for the 0.980 in. depth plates are not more than 2.3% greater than those for the 5 in. depth plates. This very small change in attenuation tends to eliminate frictional effects as an important factor in establishing the flow out of the openings for the range of parameters investigated.

Effect of Open Area on Attenuation

Figure 32 compares the average attenuation at station D for different entrance radii plates. Though there is not a common maximum attenuation point, the curves reflect the discussion of the previous results. An increase in the radius of the slot opening for the smaller values of open area will increase the attenuation; whereas, the attenuation decreases for larger open areas in the range of configurations illustrated. It is well to remember that the attenuation of the 3/8 in. radius entrance for the 2.704 square inch open area plates, 0.750 in. wide slot, would approach the value for the zero radius entrance plates as shown in Figure 30.

The points on the curves for the 0.480 square inch open area are probably high since the slot was countermilled slightly to a depth of 0.475 in. from the top which has a strong effect on the attenuation at station D. Therefore, the attenuation is probably a linear function of the open area for the illustrated configurations until the effect of the time to cross the slot width becomes dominant.

Effect of Slot With Cover Plate

The 0.400 in. wide slot with a 3/8 in. radius was chosen to determine the effect of a cover plate over the top of the opening which restricted the expansion of the gas behind the shock wave. For the three effective depths of slot test plates investigated, Table XI, the attenuation at station D was approximately 5%. The value for the 0.980 in. depth slot is close to the attenuation value of 7.7% for the open slot of same depth; whereas, the 13.6% attenuation at station D for the 0.480 in. depth slot open to the atmosphere is much greater. This correlation demonstrates the strong dependence of the station D attenuation on the time to establish the flow out.

The 10.1% attenuation at station E for the 0.480 in. depth slot test plates tends to illustrate the equalization of pressure across the shock front because the value is not much greater than the 7.2% attenuation for station E with blank test plates in the test section.

Effect of Hole Geometry

The test plates with five-0.500 diameter holes, open area equals 0.982 square inch, were investigated for possible correlation with the

0.281 in. wide slot whose open area per plate was 1.036 square inch. The attenuation for the drilled hole plates with zero and 1/8 in. entrance radius, Table XIV, was greater than those for the slotted plates, Table VI. The perforated plates had three holes upstream of the test plates midpoint on which the slots were centered; therefore, the initial flow out of these holes could more than offset the increased open area of the slotted plates.

The drilled-hole plates with 1/4 in. entrance radius showed a decrease in attenuation while the 0.281 in. slot attenuation increased linearly to this point. The strong dependence of the cylindrical reflected shock strength on the time for the incident shock wave to travel across the opening probably accounts for this lower attenuation. The effective length of the disturbance, slot width plus two times entrance radius, was 1 in. for the 0.500 in. diameter hole with 1/4 in. entrance radius; whereas, the effective length for the 0.281 in. slot with 1/4 in. entrance radius was approximately 3/4 in.. When the effective length of the disturbance for the 0.281 in. wide slot was increased to 1 in. with the 3/8 in. entrance radius, the attenuation for station D also decreased for this configuration.

Schlieren Correlation

General. Figure 22 shows representative Schlieren pictures of the shock wave passing over various slot openings. The shock wave is moving from right to left in all the Schlieren pictures of this investigation. The horizontal black strip in each picture represents

the test plate in the test section. As the shock wave passes the upstream edge of the disturbance it is normal to the inside surface of the test plate. The remaining pictures of Figure 22 have similarity in the flow pattern. The expansion flow, A in Figures 2 and 22, which appears darker than the undisturbed flow, at the start of the disturbance is evident in each picture. The cylindrical reflected shock waves, B in Figure 22, are shown as a bright intensity curved line. In each case, the portion of the shock between the reflected cylindrical wave and the test plate, C to D in Figure 22, is straight but is not normal to the test plate. The lagging of this portion behind the incident shock wave indicates a localized weakening of the shock wave.

The part of the wave between the cylindrical reflected shock wave and the undisturbed flow, D to E in Figure 22, is curved as the rarefaction waves, F in Figure 22, are in the process of reducing the shock strength. The remaining unaffected part of the shock remains normal to the test plate.

Since the transducers are mounted level with the inside surface of the test plates, the pressure rise at the downstream station D, located only 13 inches downstream of the disturbance, is probably a localized effect. The pressure rise at station E, 41 inches downstream of the disturbance, is representative of the complete shock wave which is normal to the incident flow direction when reaching this station as shown in Figure 27. The photograph, taken 8 inches upstream of station E, shows the incident shock wave parallel to a string which is perpendicular to the top and bottom walls of the shock tube.

0.400 Inch Slot With Cover Plate. Figure 23 depicts the flow phenomena when the expansion of the flow behind the shock wave is extremely limited. The picture on the right is similar to those in Figure 22. The left picture, which was taken after the shock had passed station D, shows the dissipation of the expansion fan at the upstream edge of the disturbance while the reflected compression waves are still forming.

Flow Out Open Area. Figures 24, 25 and 26 show the formation of the reflected cylindrical shock waves on the downstream edge of the opening for the 0.400 in. slot and five-0.500 in. diameter holes for equal strength incident shock waves. The localized expansion flow on the upstream edge of the disturbance and the rarefaction waves generated by the flow out of the openings are representative of the phenomena for these configurations.

The center picture in Figure 25 for the drilled-hole test plates shows the formation of an expansion flow at the upstream edge of the two rows of drilled holes.

The left picture, Fig. 26, for the countermilled 0.400 in. wide slot indicates the stability of the expansion flow at the upstream edge for a well established flow out the slot opening. The complex phenomena on the outside of the test plates is also depicted in the left Schlieren photograph.

VII. Summary of Results and Recommendations

Summary of Results

For this experimental study the following results were determined.

1) The attenuation of the shock wave in passing over the transversely slotted wall was not a function of the shock wave strength for the investigated range of pressure ratios across the shock front.

2) The attenuation and the shock strength of the incident shock wave is a function of the distance travelled, therefore the time elapsed, from the disturbance.

3) The strength of the incident shock wave downstream of a disturbance is a function of the ease with which the quasi-steady flow out through the openings is established. The following effects determine the ease in establishing the outward flow:

a) The strength of the cylindrical reflected shock waves, generated at the downstream boundary of the disturbance, is dependent on the time to traverse the slots or perforated holes by the incident shock wave. The reflected waves are formed immediately after shock wave passage.

b) A decrease in depth of the wall opening, normal to the flow direction of the incident shock front, diminishes the effect of the reflected shock waves on the ease in which the mass flow out is established.

4) The loss of mass behind the incident shock waves

generates rarefaction waves which weaken the shock wave for all configurations investigated.

5) The attenuation of the incident shock wave for a fixed open area is a function of the flow-disturbance entrance radius and the distance across the opening parallel to the incident flow. This function is non-linear for slot widths greater than approximately 0.281 inch.

6) The attenuation is a non-linear function of the open area per plate for a fixed radius of the disturbance opening.

7) The orientation of the incident shock wave is altered by the disturbance to the flow in the region behind the incident shock wave. The disturbed part of the shock wave which progresses into the shock tube travels slower than the undisturbed portion because the rarefaction waves weaken the incident shock wave. The undisturbed portion of the shock wave remains normal to the flow while the disturbed portion lags behind at a trailing angle since it is travelling slower.

Recommendations

To increase the knowledge of this complex flow interaction, it is recommended that:

1) An interferometer study with time dependent mass flow measurements be made of the effects in a slotted wall.

2) A study of perforated walls be made with various effective depth of hole openings.

VIII. Bibliography

1. Cameron, R. M. A Study of Shock Waves Moving Over a Perforated Wall. Master's Thesis, Institute of Technology (AU), August 1960.

2. Crichton, T. P. The Effect of Tube Length and Diameter on the Pressure Response of Recessed Piezoelectric Transducers. Master's Thesis, Institute of Technology (AU), September 1959.

3. Donaldson, C. and R. D. Sullivan. The Effect of Wall Friction on the Strength of Shock Waves in Tubes and Hydraulic Jumps. Technical Note 1942, National Advisory Committee for Aeronautics, 1949.

4. Eckhaus, W. On the Theory of Shock Reflection on Walls with Slots. Report F 167, Amsterdam: National Aeronautical Research Institute, July 1955.

5. Foy, J. L. Investigation of the Interaction Between a Shock Wave and a Deflagration Wave In a Flowing Hydrogen-Oxygen-Nitrogen Mixture. Master's Thesis, Institute of Technology (AU), August 1959.

6. Glass, I. I. Theory and Performance of Simple Shock Tubes. UTIA Review No. 12, Part I, Institute of Aerophysics, University of Toronto, Canada, May 1958.

7. Hall, J. G. Production of Strong Shock Waves; Shock Tube Applications, Design and Instrumentation. UTIA Review No. 12, Part II, Institute of Aerophysics, University of Toronto, Canada, May 1958.

8. Huber, P. W. and D. R. McFarland. Boundary Layer Growth and Shock Attenuation in a Shock Tube With Roughness. Technical Note 3627, National Advisory Committee for Aeronautics, 1956.

9. Shapiro, A. H. The Dynamics and Thermodynamics of Compressed Fluid Flow. Vol. II. N. Y.: The Ronald Press Co., 1954.

10. Sleator, D. B. and M. R. Lewis. A Direct Method of Measuring Density Behind Shock Waves. Report No. 1087, Ballistic Research Laboratories, December 1959.

11. Sun, T. F. On the Attenuation of a Shock From a Slotted Wall. Cornell Aeronautical Laboratories Inc. August 1953.

12. Young, A. E., S. McCullough, and R. Smith. Power Unit for a High-Intensity Light Source. RM-E-50K27, National Advisory Committee for Aeronautics, July 1951.

Table II

Transducer Calibration

Run	M_s	P_{21}	p_1	p_2-p_1	Volts Transducer		
			psia.	psi.	15	16	18
1.	1.230	1.60	14.30	8.60	0.400	0.406	0.340
2.	1.248	1.65	14.30	9.30	0.410	0.410	-
3.	1.210	1.54	14.30	7.70	0.320	0.316	-
4.	1.325	1.89	14.45	12.85	-	0.560	0.500
5.	1.335	1.91	14.45	13.15	-	0.540	0.480
6.	1.342	1.94	14.45	13.55	0.560	-	0.540
7.	1.270	1.77	14.45	11.15	0.440	-	0.400
8.	1.200	1.52	14.55	7.55	0.334	-	0.280
9.	1.194	1.50	14.45	7.15	0.320	-	0.260
10.	1.415	2.17	14.50	17.00	0.700	0.720	-
11.	1.342	1.94	14.50	13.55	0.548	0.544	-
12.	1.318	1.86	14.50	12.50	0.526	0.500	0.440
13.	1.260	1.69	14.50	9.95	0.424	0.402	0.355
14.	1.220	1.57	14.50	8.30	0.340	0.350	0.293

Table III

Attenuation Check Between Stations C and D

Run	p_1	$(p_2-p_1)_C$	p_{2C}	P_{21C}	$(p_{2C}-p_{2D})$	Z_D
	psia.	psi.	psia.		psi.	%
15.	14.40	12.60	27.00	1.877	0.22	1.7
16.	14.40	12.20	26.60	1.850	0.07	0.6
17.	14.40	13.28	27.68	1.925	0.23	1.7
18.	14.40	13.65	28.05	1.950	0.20	1.5
19.	14.40	10.60	25.00	1.738	0.20	1.9
20.	14.40	10.15	24.55	1.706	0.15	1.5
21.	14.40	10.15	24.55	1.706	0.13	1.3
22.	14.30	12.70	27.00	1.890	0.10	0.8
23.	14.30	11.43	25.73	1.802	0.10	0.9
24.	14.30	10.50	24.80	1.737	0.25	2.4
25.	14.30	8.45	22.75	1.592	0.05	0.6
26.	14.20	10.35	24.55	1.730	0.09	0.9
27.	14.20	14.60	28.80	2.028	0.17	1.2
					Average =	1.3

Table IV

Attenuation Check Between Stations C and E

Run	p_1	$(p_2-p_1)_C$	p_{2C}	P_{21C}	$(p_{2C}-p_{2E})$	Z_E
	psia.	psi.	psia.		psi.	%
28.	14.33	13.95	28.28	1.973	1.10	7.9
29.	14.33	12.50	26.83	1.872	0.77	6.2
30.	14.33	12.68	27.01	1.883	0.96	7.6
31.	14.33	11.48	25.81	1.800	0.80	6.9
32.	14.33	9.40	23.73	1.655	0.55	5.9
33.	14.33	10.90	25.23	1.760	0.88	8.0
34.	14.33	10.80	25.13	1.752	0.65	6.0
35.	14.33	10.69	25.02	1.746	0.82	7.7
36.	14.33	9.32	23.65	1.650	0.64	6.8
37.	14.33	12.20	26.53	1.850	1.03	8.4
38.	14.33	11.42	25.75	1.797	0.90	7.8
					Average =	7.2

Table V

Attenuation From 0.130 Inch Slot

0.480 $in.^2$ Open Area Per Plate

Run	Radius	p_1	$(p_2-p_1)_C$	$p_{2C}-p_{2D}$	$p_{2C}-p_{2E}$	Z_D	Z_E
	inch	psia.	psi.	psi.	psi.	%	%
39.	zero	14.30	14.23	0.58	2.95	4.1	20.7
40.	"	"	10.92	0.67	-	6.1	-
41.	"	"	11.75	0.71	-	6.0	-
42.	"	"	11.75	0.75	-	6.4	-
43.	"	14.33	10.80	0.52	-	4.8	-
44.	"	"	11.90	0.73	2.76	6.1	23.2
45.	"	"	11.95	0.78	2.81	6.5	23.5
46.	"	"	8.45	0.39	2.00	4.6	23.7
47.	"	"	9.90	0.49	2.60	5.0	26.3
48.	"	"	14.30	0.79	3.28	5.5	22.9
					Average:	5.5	23.6
49.	1/16	14.10	11.88	0.86	-	7.2	-
50.	"	"	11.40	0.70	-	6.1	-
51.	"	"	10.90	0.83	-	7.6	-
52.	"	"	11.67	0.79	-	6.8	-
53.	"	"	11.88	0.76	-	6.4	-
54.	"	"	14.02	1.22	-	8.7	-
55.	"	"	11.65	0.79	-	6.8	-
					Average:	7.1	-
56.	1/8	14.10	14.11	1.53	-	10.8	-
57.	"	"	13.68	1.58	-	11.5	-
58.	"	"	14.14	1.56	-	11.0	-
59.	"	"	13.37	1.57	-	11.7	-
60.	"	"	13.68	1.28	-	9.4	-
61.	"	"	14.01	1.56	-	11.1	-
62.	"	"	13.68	1.43	-	10.5	-
63.	"	14.33	13.97	1.52	-	10.9	-
64.	"	"	13.97	1.87	-	13.4	-
65.	"	"	14.30	1.27	-	8.9	-
66.	"	"	14.63	1.60	-	10.9	-
67.	"	"	14.11	1.53	-	10.8	-
68.	"	"	14.37	1.70	-	11.8	-
69.	"	14.40	13.97	1.35	-	9.7	-
70.	"	"	13.92	1.38	-	9.9	-
71.	"	14.30	14.86	1.44	-	9.7	-
72.	"	"	14.59	1.56	-	10.7	-
73.	"	14.27	14.11	1.53	-	10.8	-
74.	"	"	14.15	1.57	-	11.2	-
					Average:	10.7	-

Table VI

Attenuation From 0.281 Inch Slot

1.036 $in.^2$ Open Area Per Plate

Run	Radius	P_1	$(P_2-P_1)_C$	P_{2C}	$(P_{2C}-P_{2D})$	$(P_{2C}-P_{2E})$	Z_D	Z_E
	inch	psia.	psi.		psi.	psi.	%	%
75.	zero	14.23	10.45	1.733	0.67	-	6.4	-
76.	"	"	11.56	1.810	0.86	2.91	7.4	25.2
77.	"	"	13.98	1.980	0.95	2.86	6.8	20.4
78.	"	"	12.18	1.853	0.90	3.00	7.4	24.6
79.	"	"	10.90	1.764	0.79	2.77	7.2	25.4
80.	"	14.30	12.40	1.870	0.60	3.47	4.8	27.9
81.	"	"	11.28	1.790	0.65	2.78	5.8	24.6
82.	"	"	10.25	1.718	0.61	-	6.0	-
83.	"	"	9.50	1.667	0.70	2.42	7.4	25.5
84.	"	"	5.35	1.475	0.23	1.17	1.3	21.9
85.	"	"	17.44	2.225	0.92	3.81	5.3	21.8
						Average:	6.3	24.2
86.	1/16	14.10	14.14	-	1.34	-	9.5	-
87.	"	"	13.68	-	1.28	-	9.3	-
88.	"	"	14.14	-	1.18	-	8.4	-
89.	"	"	12.27	-	1.10	-	9.0	-
90.	"	"	14.14	-	1.47	-	10.4	-
91.	"	"	13.59	-	1.34	-	9.9	-
92.	"	"	14.06	-	1.10	-	7.8	-
93.	"	"	13.78	-	1.21	-	8.8	-
						Average:	9.1	-
94.	1/8	14.10	13.82	1.980	1.84	3.48	13.3	25.2
95.	"	"	13.68	1.970	1.68	3.56	12.3	26.0
96.	"	"	17.91	2.270	1.88	6.10	10.5	34.0
97.	"	"	19.55	2.395	2.35	5.90	12.0	30.2
98.	"	"	19.90	2.412	2.67	6.25	13.4	31.4
99.	"	"	16.28	2.155	1.61	4.68	9.9	28.8
100.	"	"	12.74	1.905	1.42	2.68	11.3	29.0
101.	"	"	8.73	1.620	0.83	2.46	9.5	27.8
102.	"	"	8.96	1.637	1.20	2.16	13.4	24.1
103.	"	"	7.87	1.525	0.85	2.07	11.5	28.1
						Average:	11.7	28.6

Continued:

Table VI Continued

Run	Radius	p_1	$(p_2-p_1)_C$	P_{21C}	$P_{2C}-P_{2D}$	$P_{2C}-P_{2E}$	Z_D	Z_E
	inch	psia.	psi.		psi.	psi.	%	%
104.	1/4	14.32	13.88	-	2.28	-	16.4	-
105.	"	"	13.88	-	2.51	-	18.0	-
106.	"	"	14.00	-	2.35	-	16.8	-
107.	"	"	13.74	-	2.28	-	16.6	-
108.	"	"	13.42	-	2.09	-	15.6	-
109.	"	"	11.52	-	2.06	-	17.9	-
						Average:	16.9	-
110.	3/8	14.30	14.15	-	1.90	-	13.4	-
111.	"	"	13.78	-	2.23	-	16.2	-
112.	"	"	13.78	-	1.71	-	12.4	-
113.	"	"	13.78	-	2.32	-	16.8	-
114.	"	"	13.74	-	1.74	-	12.7	-
115.	"	"	13.88	-	1.88	-	13.5	-
116.	"	"	13.92	-	2.32	-	16.7	-
						Average:	14.5	-
117.	3/8	14.30	14.02	-	-	3.40	-	24.2
118.	"	"	13.65	-	-	3.33	-	24.4
119.	"	"	13.50	-	-	3.33	-	24.7
120.	"	"	13.68	-	-	3.79	-	27.7
121.	"	"	13.60	-	-	3.20	-	23.5
122.	"	"	13.60	-	-	3.58	-	26.3
123.	"	"	13.55	-	-	3.66	-	27.0
						Average:	-	25.4

Table VII

Attenuation From 0.400 Inch Slot

1.469 $in.^2$ Open Area Per Plate

Run	Radius inch	p_1 psia.	$(p_2-p_1)_C$ psi.	$p_{2C}-p_{2D}$ psi.	$p_{2C}-p_{2E}$ psi.	Z_D %	Z_E %
124.	zero	14.20	13.60	2.14	-	15.7	-
125.	"	"	11.90	1.82	-	15.3	-
126.	"	"	12.02	1.94	-	16.0	-
127.	"	"	13.55	2.23	3.33	16.4	24.6
128.	"	"	11.95	1.59	-	13.3	-
129.	"	"	13.68	2.13	-	15.6	-
130.	"	"	13.33	1.93	-	14.5	-
131.	"	"	12.42	-	2.98	-	24.0
132.	"	14.12	12.47	-	3.03	-	24.3
133.	"	"	13.74	-	4.03	-	29.3
134.	"	"	13.68	-	3.72	-	27.2
135.	"	"	13.74	-	3.62	-	26.3
136.	"	"	14.07	-	3.89	-	27.7
					Average:	15.3	26.2
137.	1/16	14.10	14.02	2.10	4.19	15.0	29.9
138.	"	"	14.02	1.92	3.80	13.7	27.1
139.	"	"	14.67	2.42	4.45	16.5	30.4
140.	"	"	14.07	2.10	-	15.0	-
141.	"	"	13.65	2.28	4.07	16.7	29.8
142.	"	"	13.74	2.14	4.30	15.6	31.2
143.	"	"	13.60	-	4.65	-	34.2
144.	"	"	13.68	-	4.73	-	34.6
					Average:	15.4	31.0
145.	1/8	14.38	14.44	2.47	3.82	17.1	26.5
146.	"	"	14.63	2.05	3.61	14.0	24.6
147.	"	"	14.78	2.20	4.29	14.9	29.0
148.	"	"	14.63	2.14	3.88	14.6	26.5
149.	"	"	14.63	2.43	4.14	16.6	28.3
150.	"	"	14.63	2.09	4.41	14.3	30.1
					Average:	15.3	27.5

Continued:

Table VII Continued

Run	Radius	p_1	$(p_2-p_1)_C$	$p_{2C}-p_{2D}$	$p_{2C}-p_{2E}$	Z_D	Z_E
	inch	psia.	psi.	psi.	psi.	%	%
151.	1/4	14.39	14.63	1.60	-	10.9	-
152.	"	"	14.02	1.35	-	9.6	-
153.	"	"	14.02	1.53	-	10.9	-
154.	"	"	14.39	1.20	-	8.3	-
155.	"	"	14.07	1.17	-	8.3	-
156.	"	"	14.15	1.57	-	11.1	-
157.	"	"	14.15	0.96	-	6.8	-
					Average:	9.4	-
158.	3/8	14.32	13.74	1.16	-	8.4	-
159.	"	"	13.45	0.87	-	6.5	-
160.	"	"	13.55	1.06	-	7.8	-
161.	"	"	13.68	1.01	-	7.4	-
162.	"	"	13.60	1.11	-	8.2	-
163.	"	"	13.60	1.15	-	8.5	-
164.	"	"	13.68	1.01	-	7.4	-
					Average:	7.7	-

Table VIII

Attenuation From 0.400 Inch Slot With 4 Inch Slot Extension
(1.469 in.^{2} Open Area Per Plate)

Run	Radius	P_1	$(P_2-P_1)_C$	$P_{2C}-P_{2D}$	$P_{2C}-P_{2E}$	Z_D	Z_E
	inch	psia.	psi.	psi.	psi.	%	%
165.	zero	14.30	14.15	2.05	3.93	14.5	27.8
166.	"	"	14.15	1.75	3.13	12.4	22.1
167.	"	"	13.55	1.71	2.80	12.6	20.7
168.	"	"	13.90	1.79	3.41	12.9	24.5
169.	"	"	14.39	1.81	3.11	12.6	21.6
170.	"	"	13.96	1.80	2.94	12.9	21.1
					Average:	13.0	23.0
171.	1/16	14.10	14.15	1.95	3.66	13.8	25.9
172.	"	"	13.92	1.85	3.57	13.3	25.6
173.	"	"	13.21	1.56	3.50	11.8	26.5
174.	"	"	14.30	1.90	4.34	13.3	30.3
175.	"	"	14.15	2.05	4.19	14.5	29.6
176.	"	"	13.55	1.86	3.72	13.7	27.5
					Average:	13.4	27.6
177.	1/8	14.38	14.67	2.09	4.05	14.2	27.6
178.	"	"	14.39	1.81	3.90	12.6	27.1
179.	"	"	14.78	1.75	3.76	11.8	25.4
180.	"	"	14.63	1.83	3.61	12.5	24.6
181.	"	"	14.63	2.09	4.14	14.3	28.3
182.	"	"	14.50	2.17	4.54	15.0	31.3
					Average:	13.4	27.6
183.	1/4	14.41	13.78	1.24	-	9.0	-
184.	"	"	13.68	1.10	-	8.1	-
185.	"	"	13.17	1.07	-	8.1	-
186.	"	"	13.74	0.88	-	6.4	-
187.	"	"	13.55	1.25	-	9.2	-
188.	"	"	13.88	0.88	-	6.3	-
189.	"	"	13.68	1.35	-	9.9	-
190.	"	"	14.25	1.35	-	9.5	-
					Average:	8.3	-
191.	3/8	14.32	14.22	0.98	-	6.9	-
192.	"	"	14.54	1.21	-	8.3	-
193.	"	"	13.74	1.16	-	8.4	-
194.	"	"	13.45	0.91	-	6.8	-
195.	"	"	13.65	1.03	-	7.6	-
196.	"	"	13.45	0.78	-	5.8	-
197.	"	"	13.60	1.02	-	7.5	-
					Average:	7.3	-

Table IX

Attenuation From 0.400 Inch Slot-$\frac{3}{8}$ Inch Radius
and Countermilled 1.500 Inches Wide
(1.469 $in.^2$ Open Area)

Run	Slot Depth inch	p_1 psia.	$(p_2-p_1)_C$ psi.	$(p_{2C}-p_{2D})$ psi.	Z_D %
198.	0.730	14.30	13.68	1.48	10.8
199.	"	"	13.74	1.49	10.8
200.	"	"	13.42	1.32	9.8
201.	"	"	13.60	1.63	12.0
202.	"	"	13.82	1.52	11.0
203.	"	"	14.22	1.73	12.2
204.	"	"	12.02	1.40	11.6
				Average:	11.2
205.	0.480	14.43	13.78	1.78	12.9
206.	"	"	14.11	1.81	12.8
207.	"	"	14.07	1.97	14.0
208.	"	"	14.07	1.97	14.0
209.	"	"	13.82	1.72	12.5
210.	"	"	13.78	1.81	13.1
211.	"	"	13.78	1.98	14.4
212.	"	"	13.97	2.05	14.7
				Average:	13.6

Table X

Attenuation vs. Effective Slot Depth
For 0.400 Inch Slot - 3/8 Inch Radius
(1.469 $in.^2$ Open Area)

Effective Slot Depth inch	Z_D %
5	7.3
0.980	7.7
0.730	11.2
0.480	13.6

Table XI

Attenuation From 0.400 Inch Slot - 3/8 Inch Radius

With Cover Plate Over Slot

Run	Slot Depth inch	p_1 psia.	$(p_2-p_1)_C$ psi.	$p_{2C}-p_{2D}$ psi.	$p_{2C}-p_{2E}$ psi.	Z_D %	Z_E %
213.	0.480	14.43	13.78	0.75	-	5.4	-
214.	"	"	13.68	0.44	-	3.2	-
215.	"	"	13.55	0.85	-	6.3	-
216.	"	"	13.60	0.57	-	4.2	-
217.	"	"	13.68	0.86	-	6.3	-
218.	"	"	13.78	0.92	-	6.7	-
219.	"	"	13.88	0.74	-	5.3	-
					Average:	5.3	-
220.	0.480	14.38	13.78	-	1.20	-	8.7
221.	"	"	13.45	-	1.48	-	11.0
222.	"	"	14.44	-	1.77	-	12.2
223.	"	"	13.92	-	1.62	-	11.6
224.	"	"	13.60	-	0.98	-	7.2
225.	"	"	13.92	-	1.02	-	7.3
226.	"	"	13.68	-	1.58	-	11.5
227.	"	"	13.74	-	1.54	-	11.2
						Average:	10.1
228.	0.730	14.30	13.88	0.64	-	4.6	-
229.	"	"	13.78	0.41	-	3.0	-
230.	"	"	13.88	0.74	-	5.3	-
231.	"	"	13.78	0.75	-	5.4	-
232.	"	"	13.74	0.74	-	5.4	-
233.	"	"	13.65	0.85	-	6.2	-
234.	"	"	13.68	0.78	-	5.7	-
					Average:	5.1	-
235.	0.980	14.32	13.21	0.45	-	3.4	-
236.	"	"	13.68	0.78	-	5.7	-
237.	"	"	13.82	0.63	-	4.6	-
238.	"	"	13.92	0.96	-	6.9	-
239.	"	"	14.02	0.42	-	3.0	-
240.	"	"	14.07	0.70	-	5.0	-
241.	"	"	13.82	0.63	-	4.6	-
					Average:	4.7	-

Table XII

Attenuation From 0.508 Inch Slot

1.844 $in.^2$ Open Area

Run	Radius	P_1	$(P_2-P_1)_C$	$P_{2C}-P_{2D}$	Z_D
	inch	psia.	psi.	psi.	%
242.	zero	14.31	14.96	2.99	20.0
243.	"	"	14.02	2.50	17.8
244.	"	"	15.09	2.99	19.8
245.	"	"	14.86	2.94	19.8
246.	"	"	14.37	2.49	17.3
247.	"	"	14.37	2.72	18.9
248.	"	"	14.50	2.70	18.6
249.	"	"	13.97	2.69	19.2
				Average:	18.9
250.	1/16	14.33	14.86	1.59	10.6
251.	"	"	14.78	1.36	9.2
252.	"	"	14.78	1.36	9.2
253.	"	"	14.63	1.67	11.4
254.	"	"	14.67	1.64	11.2
255.	"	"	14.59	1.32	9.1
256.	"	"	13.78	1.45	10.5
				Average:	11.9
257.	1/8	14.37	14.63	1.13	7.7
258.	"	"	14.63	1.21	8.3
259.	"	"	14.73	1.13	7.7
260.	"	"	15.20	1.56	10.3
261.	"	"	14.02	0.99	7.1
262.	"	"	14.30	1.30	9.1
263.	"	"	13.97	1.52	10.9
264.	"	"	14.15	1.45	10.2
				Average:	8.9

Continued:

Table XII Continued

Run	Radius	p_1	$(p_2-p_1)_C$	$p_{2C}-p_{2D}$	Z_D
	inch	psia.	psi.	psi.	%
265.	1/4	14.30	13.78	1.24	9.0
266.	"	"	13.65	0.62	4.5
267.	"	"	13.55	0.69	5.1
268.	"	"	13.65	1.20	8.8
269.	"	"	13.65	0.75	5.5
270.	"	"	12.97	0.67	5.2
271.	"	"	13.68	1.06	7.8
272.	"	"	13.97	1.30	9.3
				Average :	6.9
273.	3/8	14.28	14.54	1.58	10.9
274.	"	"	14.25	1.49	10.5
275.	"	"	13.88	1.30	9.4
276.	"	"	14.44	1.68	11.6
277.	"	"	14.37	1.79	12.5
278.	"	"	14.50	1.60	11.0
279.	"	"	14.63	1.87	12.8
				Average:	11.2

Table XIII

Attenuation From 0.750 Inch Slot

2.704 $in.^2$ Open Area

Run	Radius	p_1	$(p_2-p_1)_C$	$p_{2C}-p_{2D}$	Z_D
	inch	psia.	psi.	psi.	%
280.	zero	14.32	14.39	1.53	10.6
281.	"	"	14.73	1.46	9.9
282.	"	"	14.15	1.57	11.1
283.	"	"	14.54	1.96	13.5
284.	"	"	14.44	1.64	11.4
285.	"	"	14.54	1.74	12.0
286.	"	"	14.39	1.53	10.6
				Average:	11.3
287.	1/16	14.38	14.63	1.03	7.0
288.	"	"	14.59	1.09	7.5
289.	"	"	14.30	0.84	5.9
290.	"	"	14.50	1.23	8.5
291.	"	"	14.39	1.36	9.4
292.	"	"	14.44	1.02	7.1
293.	"	"	14.67	1.12	7.7
				Average:	7.6
294.	1/8	14.32	14.54	1.04	7.2
295.	"	"	14.73	1.00	6.8
296.	"	"	13.45	0.75	5.6
297.	"	"	13.92	0.89	6.4
298.	"	"	13.88	0.80	5.8
299.	"	"	14.59	1.13	7.8
300.	"	"	13.65	0.98	7.2
301.	"	"	13.82	1.02	7.4
				Average:	6.8
302.	1/4	14.22	13.45	1.35	10.0
303.	"	"	13.92	1.02	7.3
304.	"	"	13.74	1.29	9.4
305.	"	"	13.92	1.25	9.0
306.	"	"	13.65	1.32	9.7
307.	"	"	13.65	0.98	7.2
308.	"	"	13.92	1.12	8.0
				Average:	8.8

Continued:

Table XIII Continued

Run	Radius	p_1	$(p_2-p_1)_C$	$p_{2C}-p_{2D}$	Z_D
	inch	psia.	psi.	psi.	%
309.	3/8	14.28	14.07	1.31	9.3
310.	"	"	14.02	1.82	13.0
311.	"	"	14.39	1.72	11.9
312.	"	"	14.37	1.57	10.9
313.	"	"	14.25	1.22	8.6
314.	"	"	14.15	1.48	10.5
315.	"	"	14.50	1.83	12.6
				Average:	11.0

Table XIV

Attenuation From 5-0.500 Inch Diameter Holes

0.982 $in.^2$ Open Area

Run	Radius	p_1	$(p_2-p_1)_C$	$p_{2C}-p_{2D}$	$p_{2C}-p_{2E}$	Z_D	Z_E
	inch	psia.	psi.	psi.	psi.	%	%
316.	zero	14.33	14.25	1.29	2.82	9.1	19.8
317.	"	"	12.10	1.10	2.80	9.1	23.1
318.	"	"	12.02	1.07	2.76	8.9	23.0
319.	"	"	10.96	0.98	2.56	8.9	23.4
320.	"	"	8.82	0.80	2.92	9.1	23.1
321.	"	"	11.48	1.23	3.28	10.7	28.6
322.	"	"	11.05	1.27	2.99	11.5	27.1
					Average:	9.6	25.4
323.	1/8	14.17	14.96	2.10	-	14.1	-
324.	"	"	14.54	1.87	-	12.9	-
325	"	"	14.02	1.69	-	12.1	-
326.	"	"	13.37	1.57	-	11.8	-
327.	"	"	14.39	2.14	-	14.9	-
328.	"	"	14.86	2.24	-	15.1	-
					Average:	13.5	-
329.	1/4	14.32	13.92	0.89	-	6.4	-
330.	"	"	14.67	1.07	-	7.3	-
331.	"	"	14.67	1.21	-	8.3	-
332.	"	"	14.25	1.11	-	7.8	-
333.	"	"	14.78	1.41	-	9.5	-
334.	"	"	14.54	1.40	-	9.6	-
335.	"	"	14.39	1.02	-	7.6	-
336.	"	"	14.15	1.35	-	9.5	-
					Average:	8.3	-

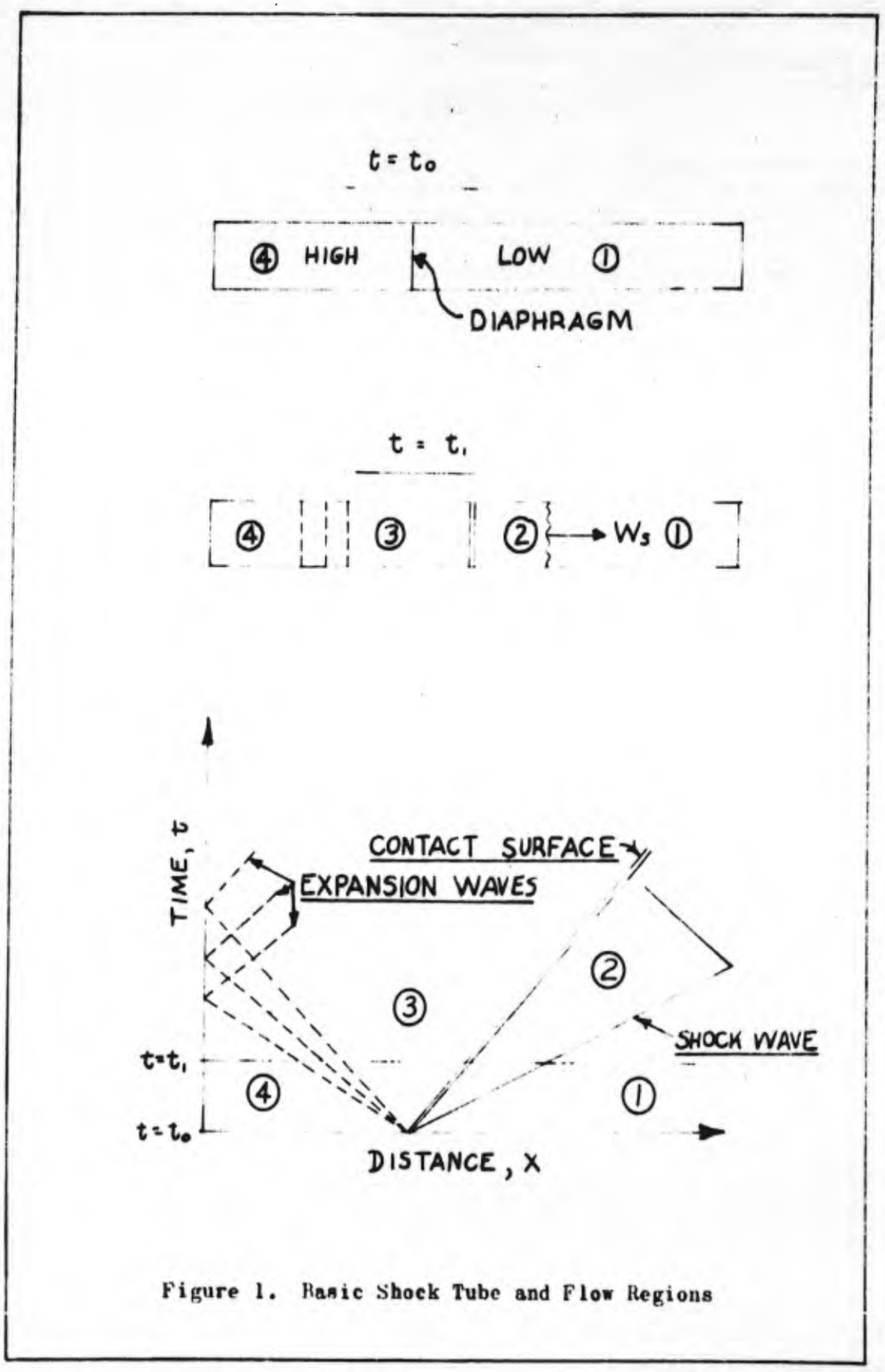

Figure 1. Basic Shock Tube and Flow Regions

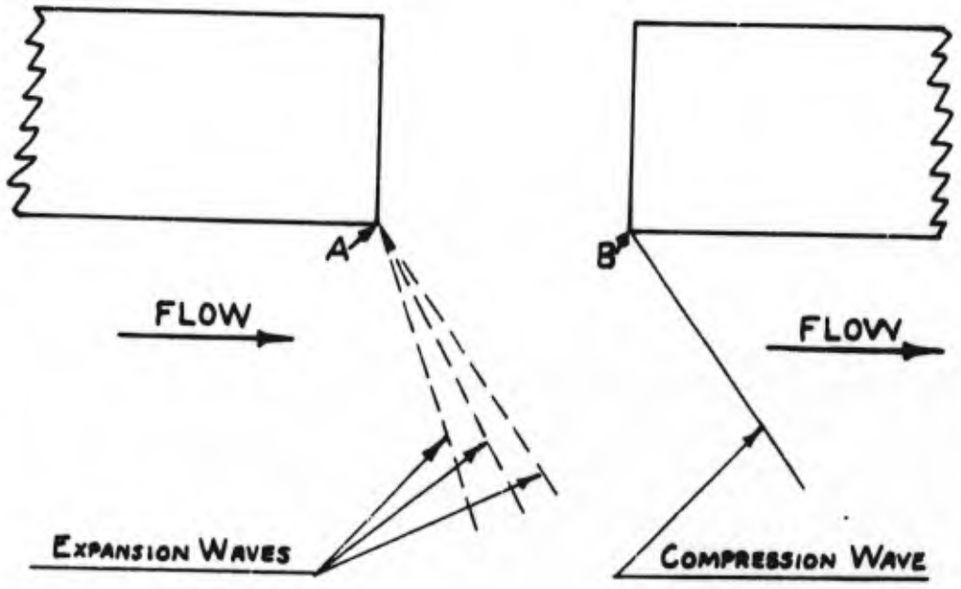

Figure 2. Parallel Flow Across an Opening

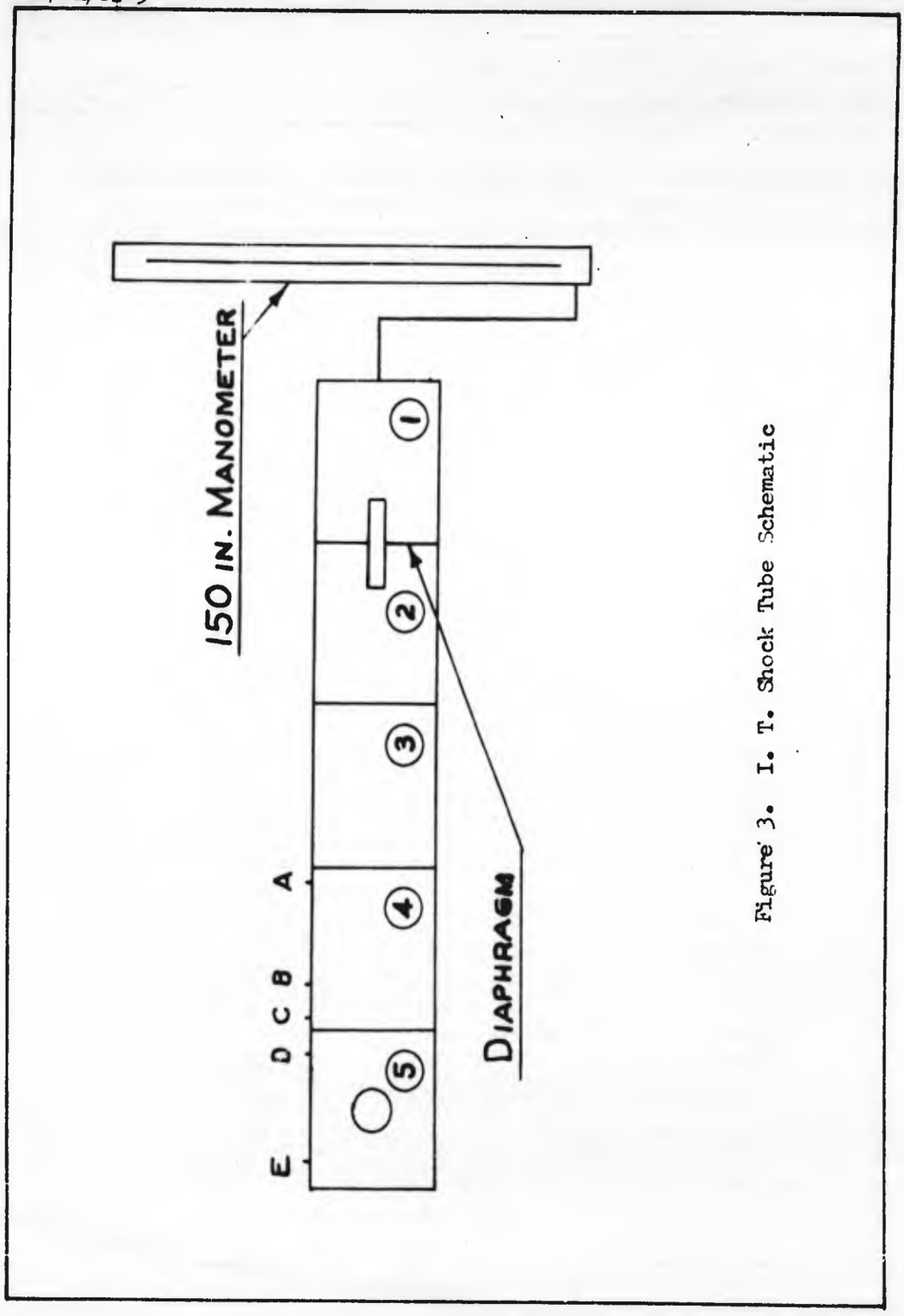

Figure 3. I. T. Shock Tube Schematic

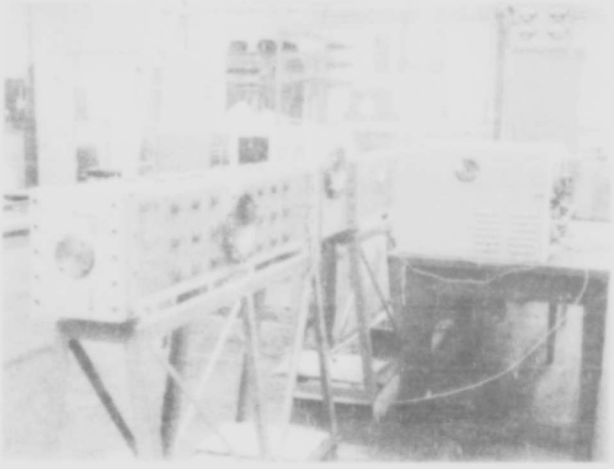

View From Section 5 End

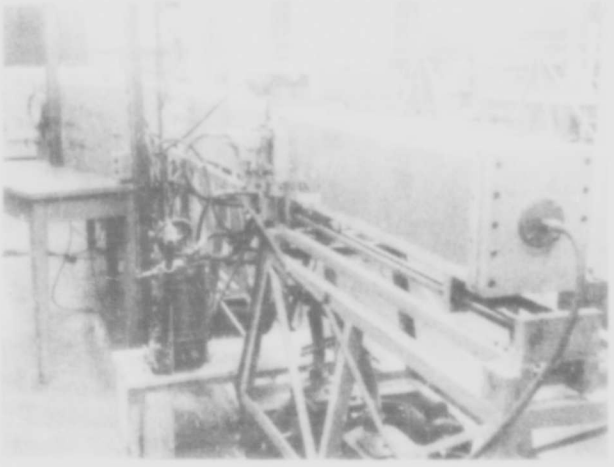

View From Section 1 End

Figure 4. General View of Shock Tube

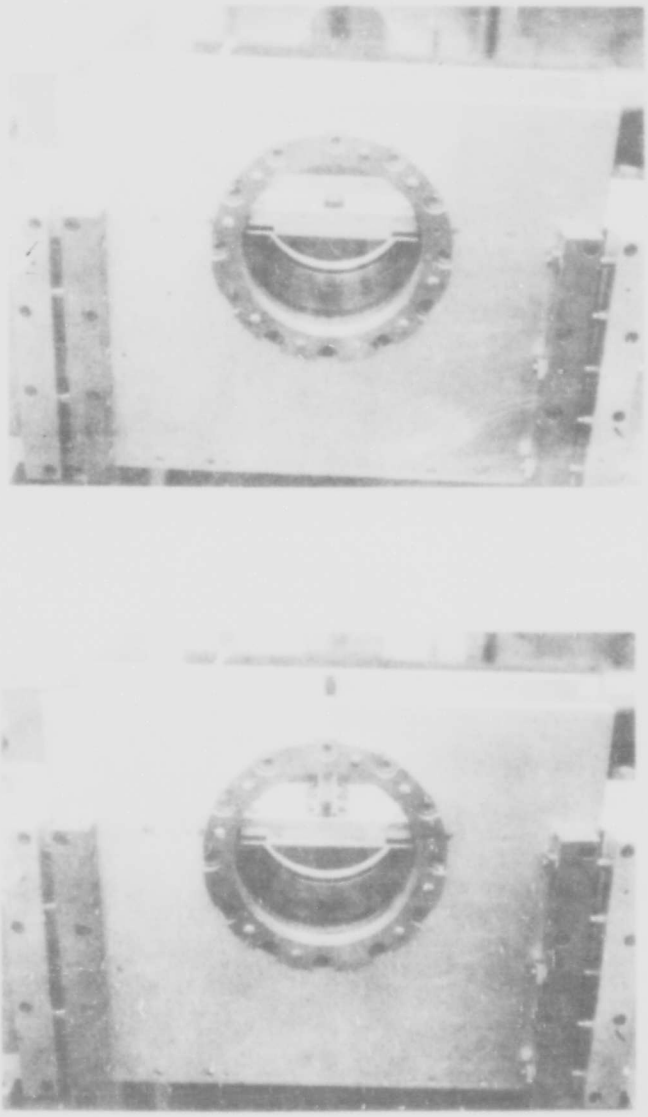

Figure 5. General View of Test Section

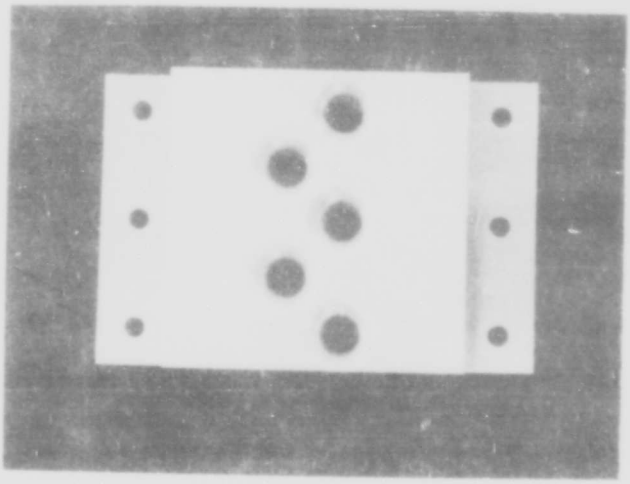

Figure 6. Test Plate With 5-0.500 In. Diameter Holes

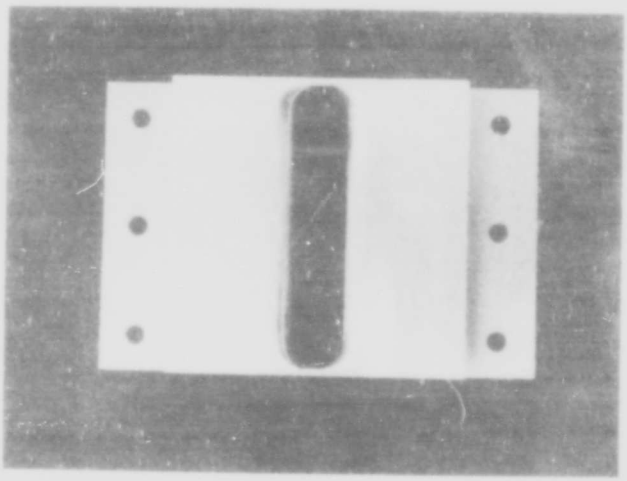

Figure 7. Test Plate With 0.750 In. Slot- 3/8 In. Radius

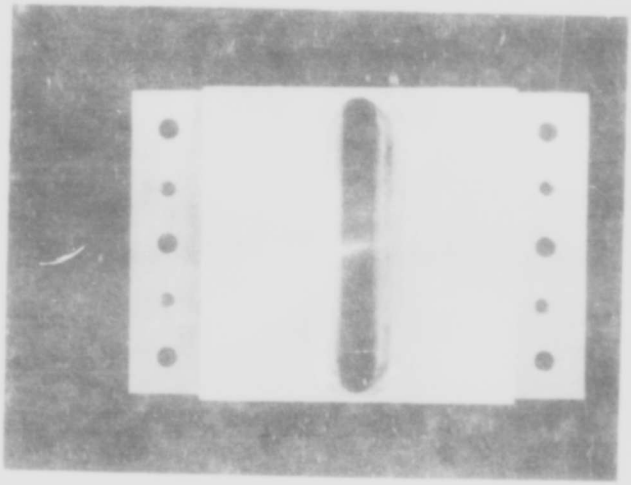

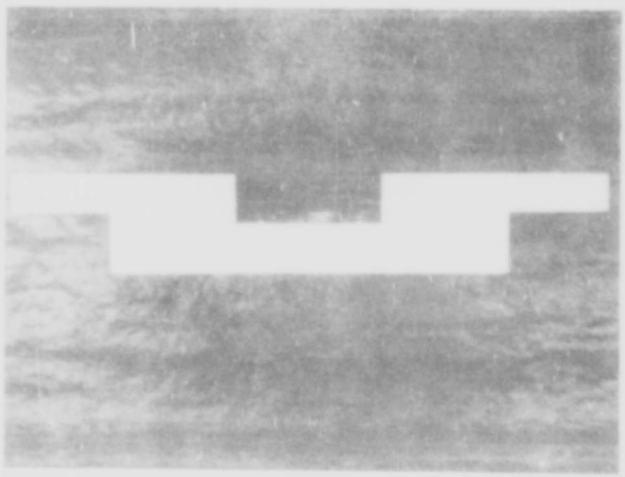

Figure 8. Test Plates With 0.400Inch Slot

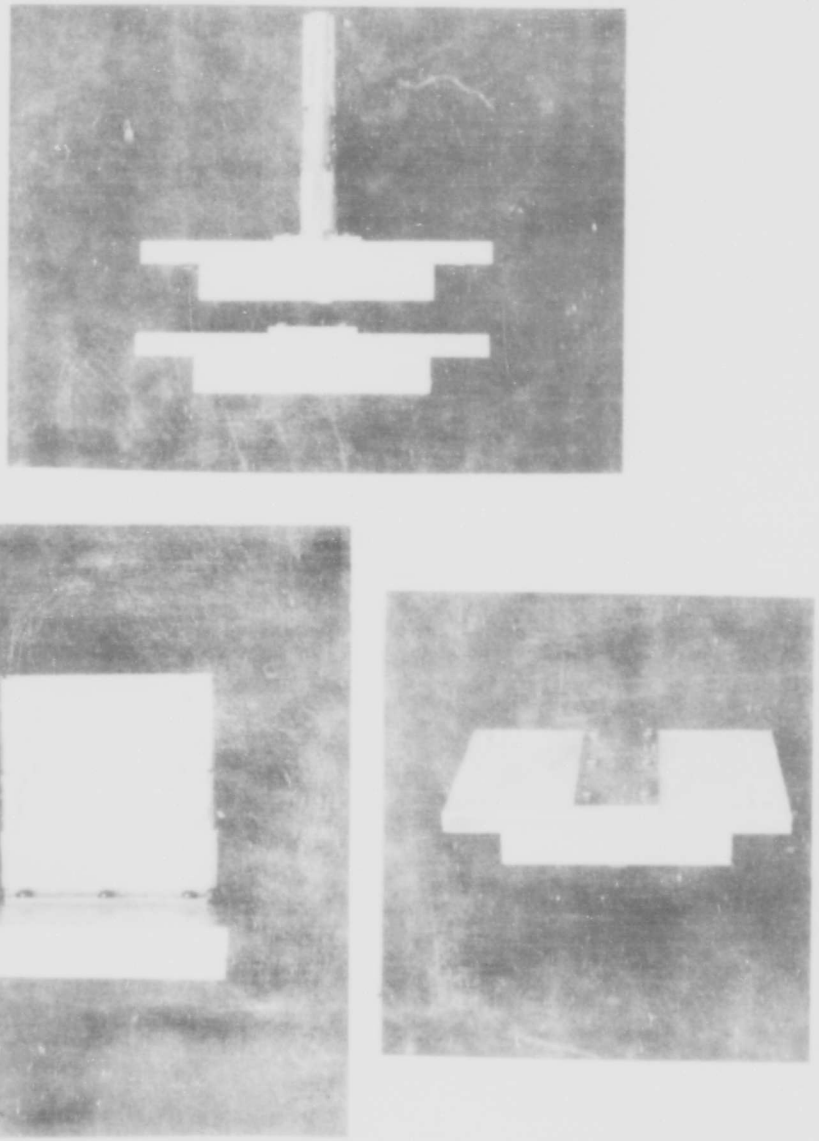

Figure 9. 0.400 In. Slot Test Plates with Slot Extensions and Cover Plates

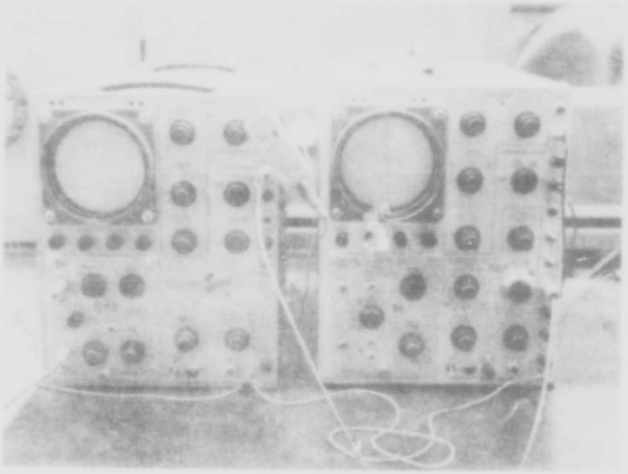

Figure 10. Type 531 and 1805 Oscilloscopes

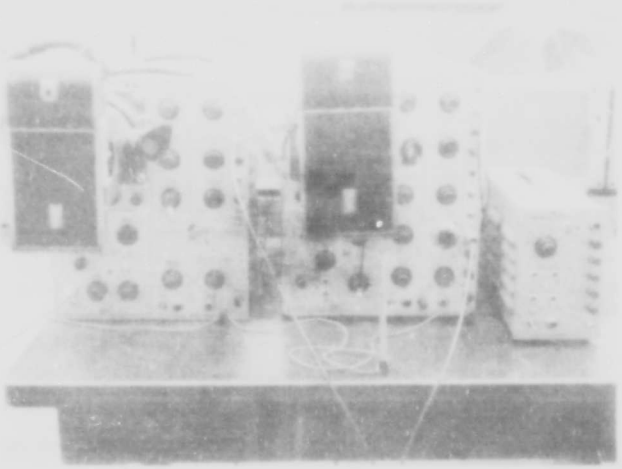

Figure 11. Oscilloscope Cameras Mounted and Time Mark Generator

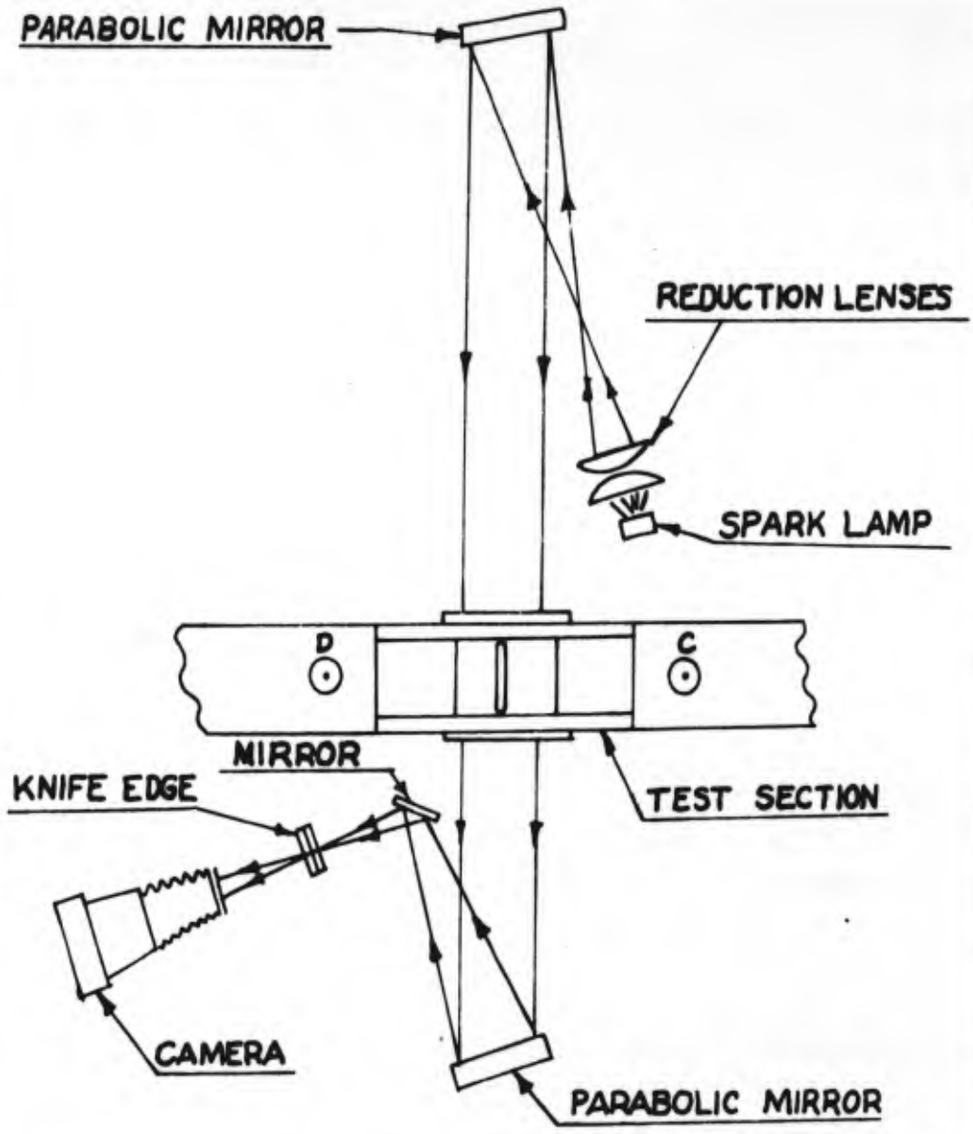

Figure 12. Schlieren System Photographic Schematic

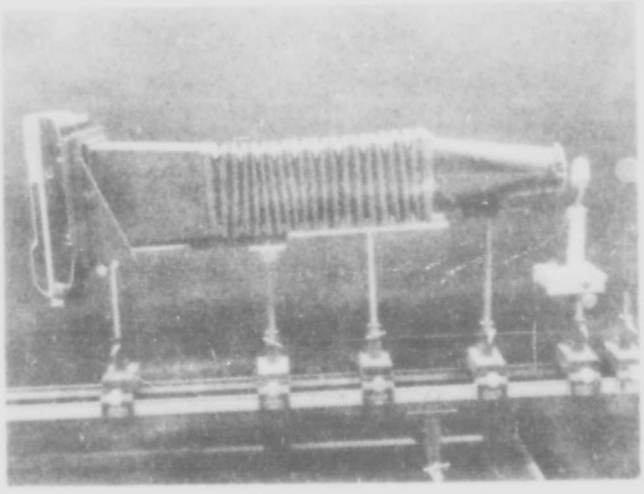

Figure 13. Schlieren System Camera, Bellows, Knife Edge and Mirror

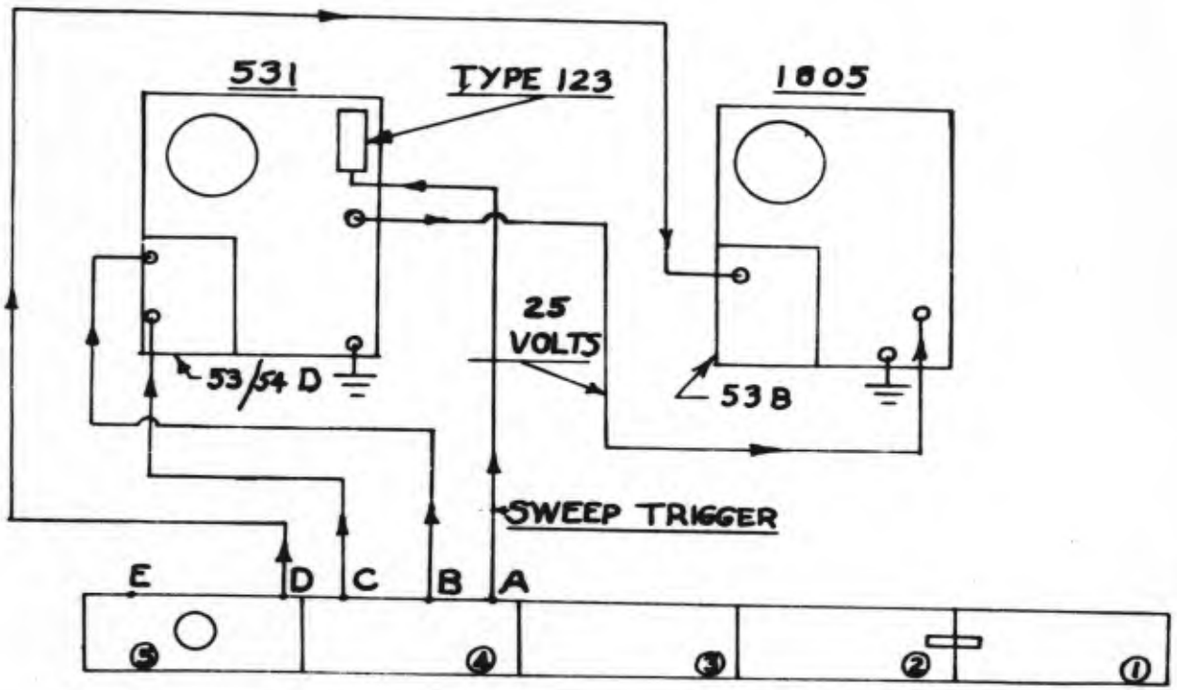

Figure 14. Transducer Calibration Configuration Schematic

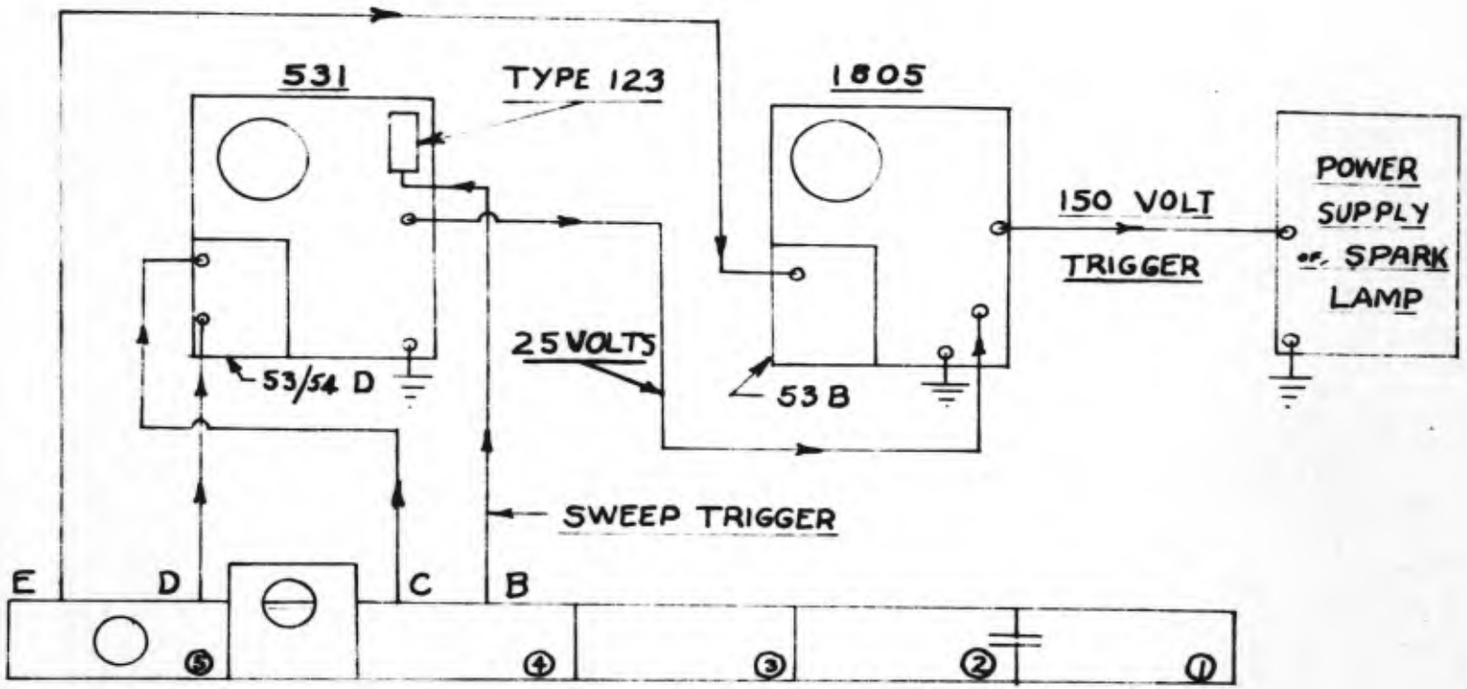

Figure 15. Experimental Run Configuration Schematic

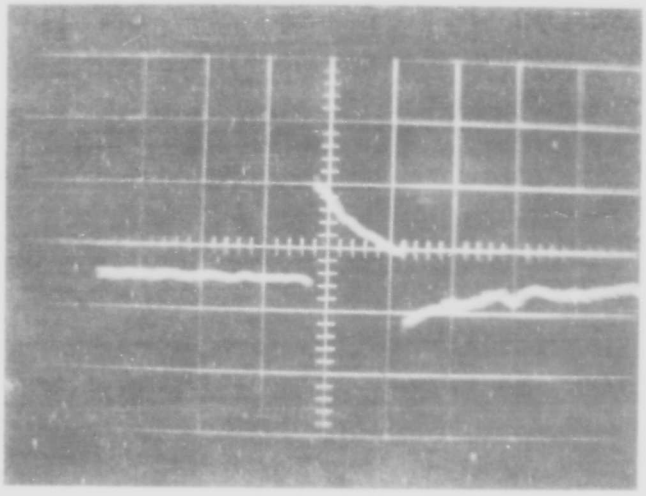

Figure 16. Oscilloscope Picture During Transducer Calibration

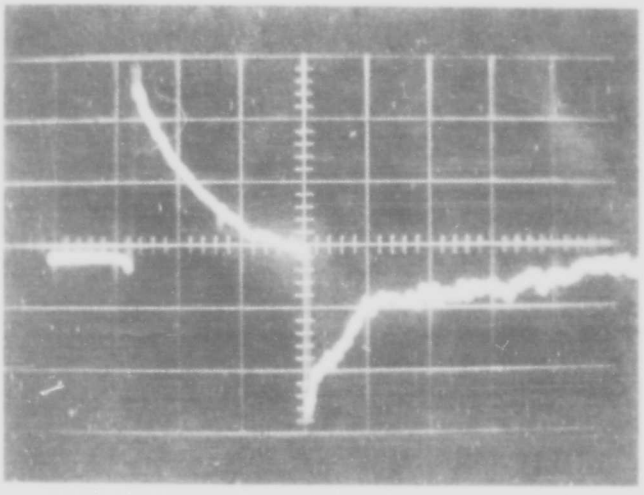

Figure 17. Oscilloscope Picture During Experimental Runs

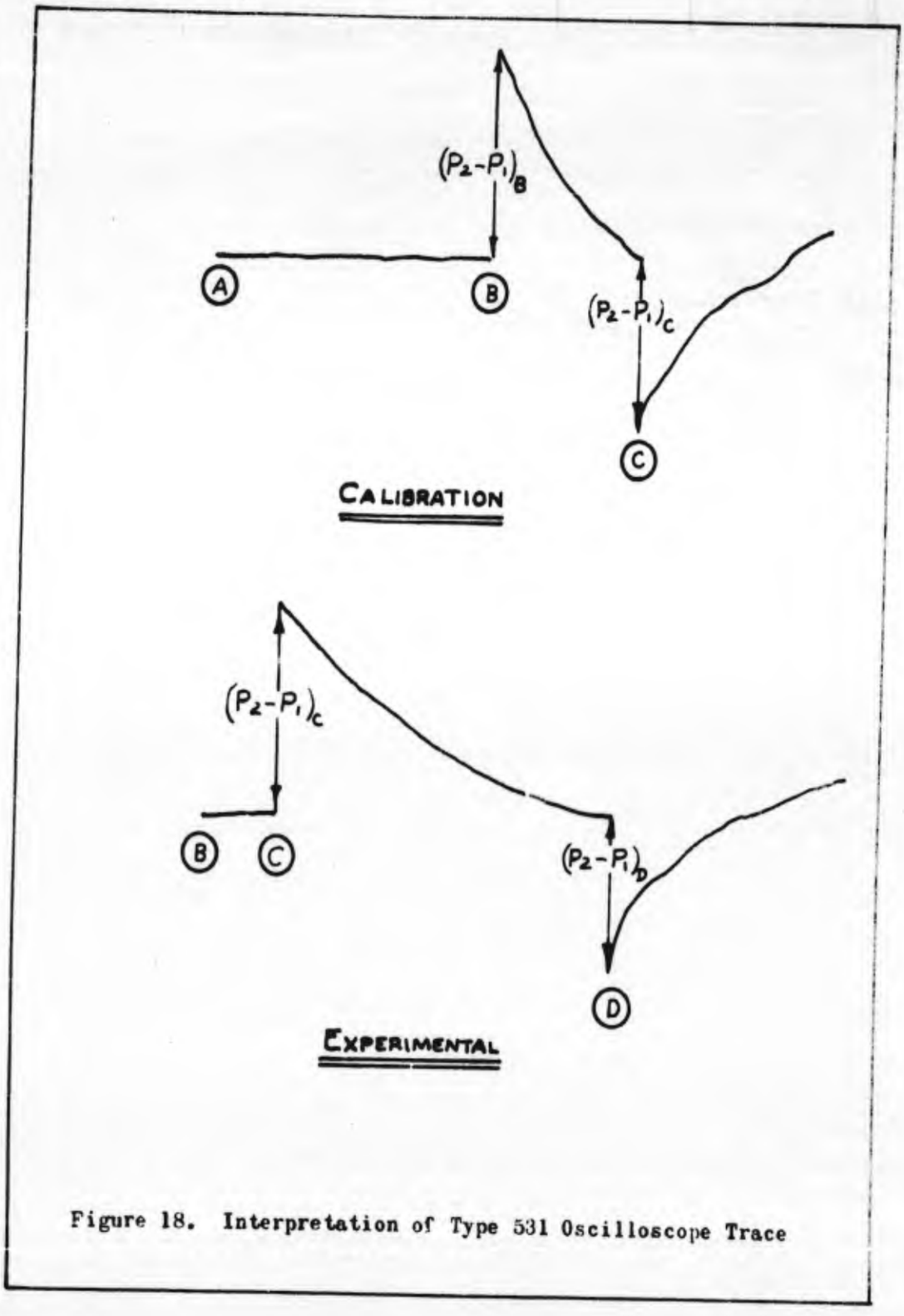

Figure 18. Interpretation of Type 531 Oscilloscope Trace

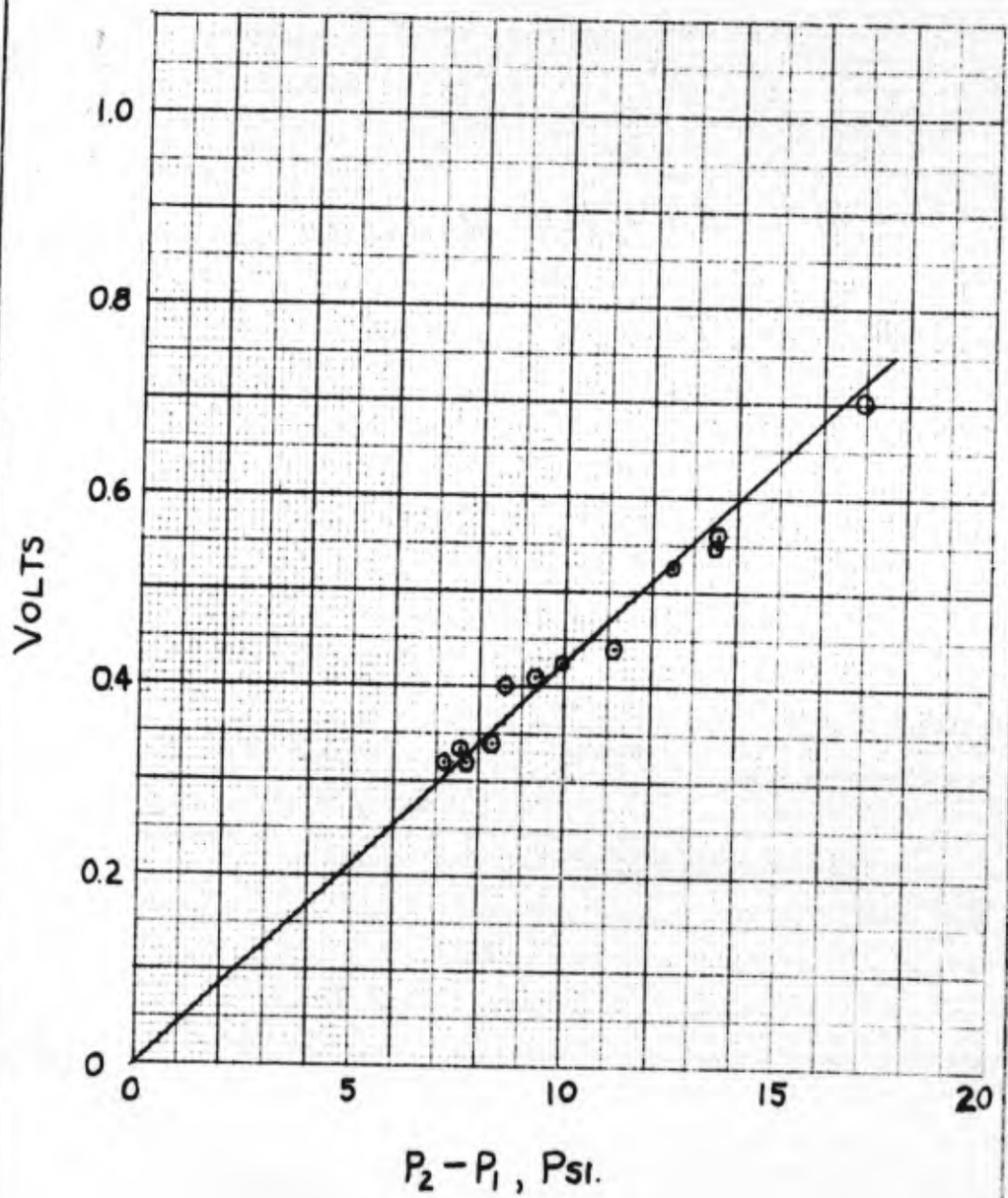

Figure 19. Transducer #15 Calibration Curve

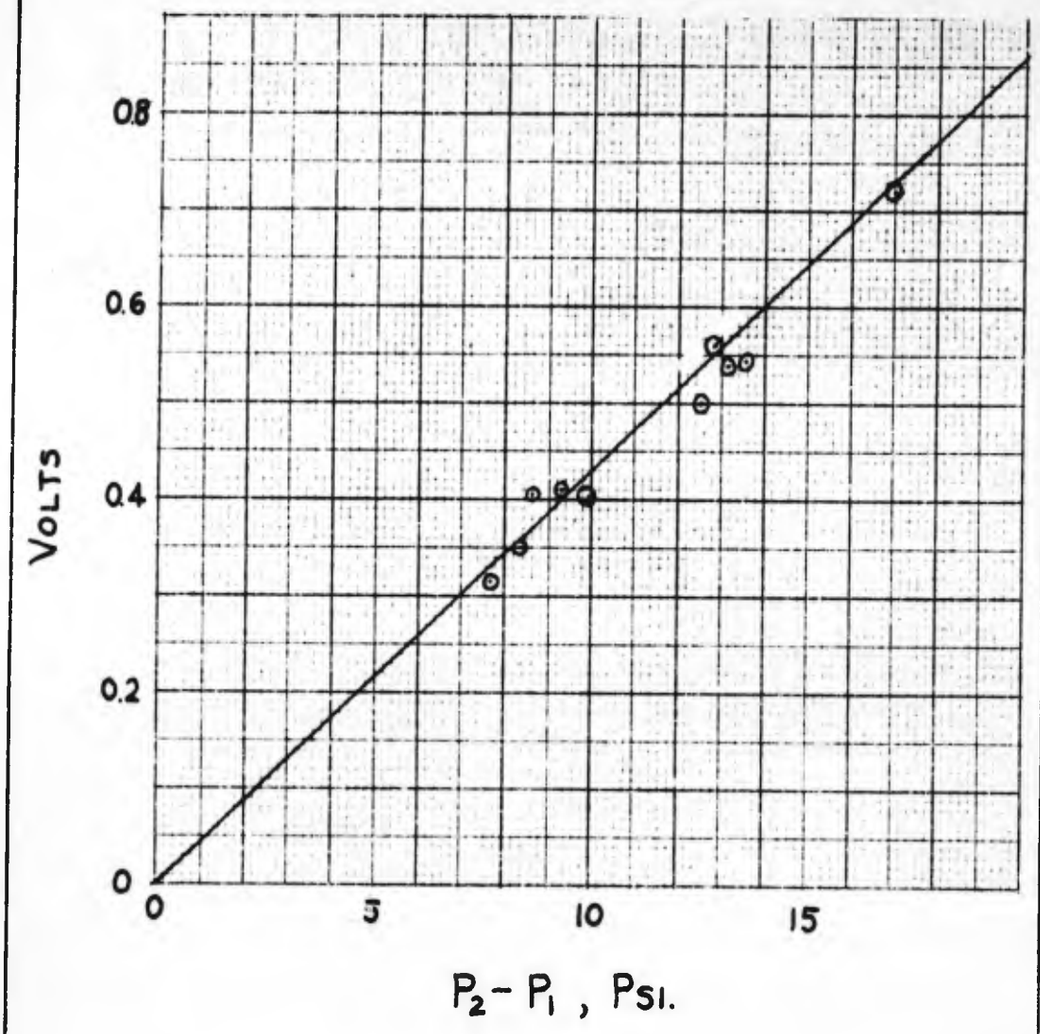

Figure 20. Transducer #16 Calibration Curve

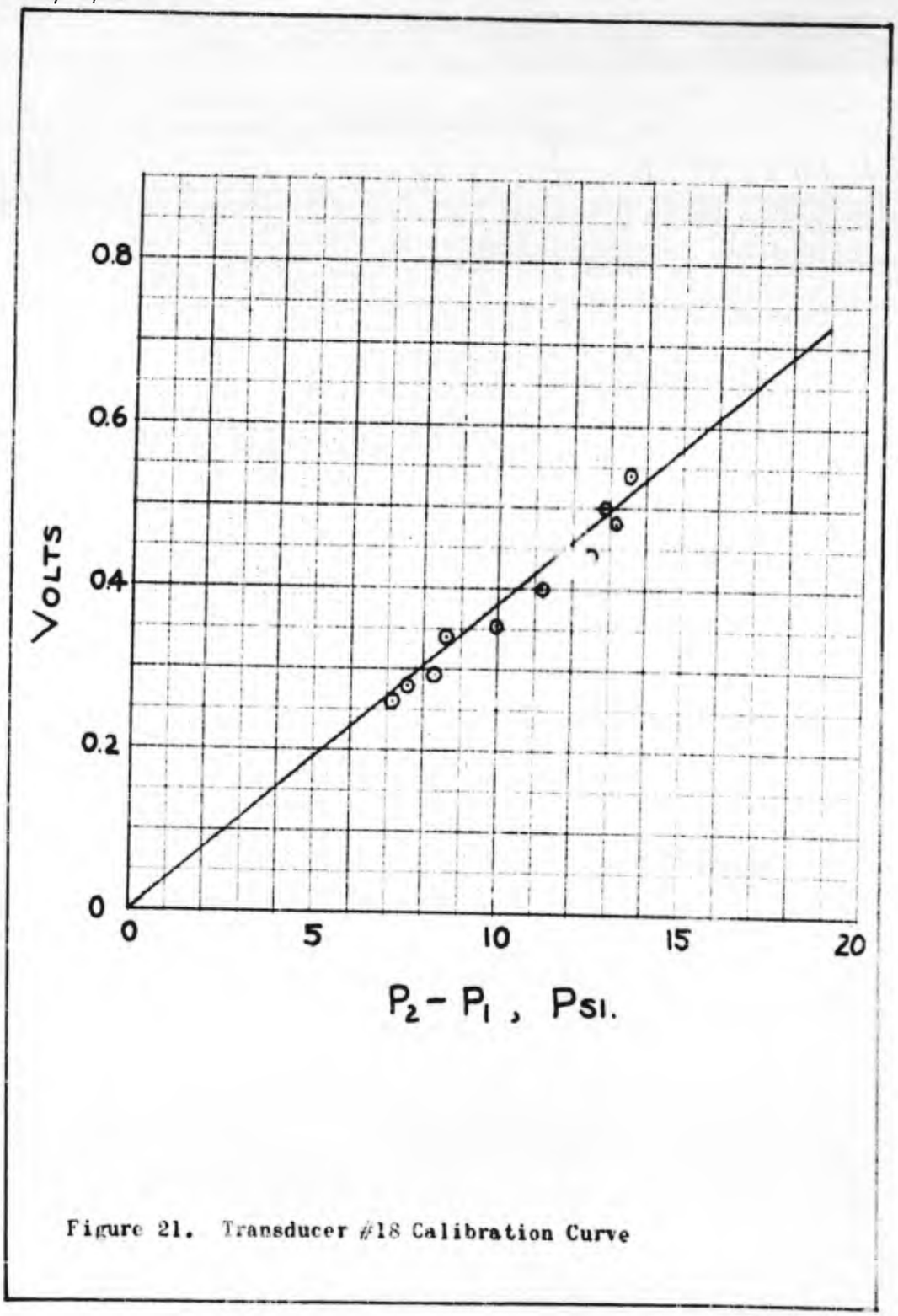

Figure 21. Transducer #18 Calibration Curve

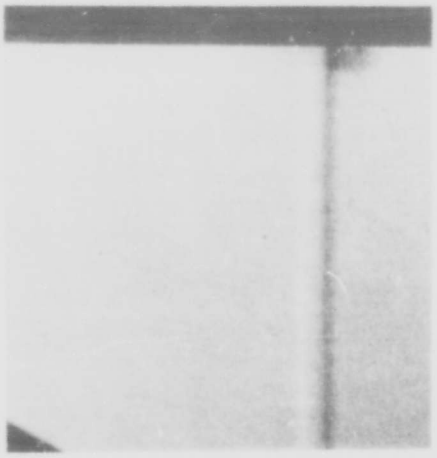

Shock at Start of Slot

0.130 In. Slot- 1/8 In. Radius

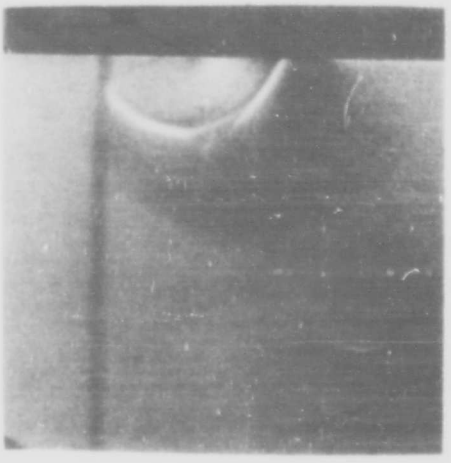

0.508 In. Slot- 1/8 In. Radius

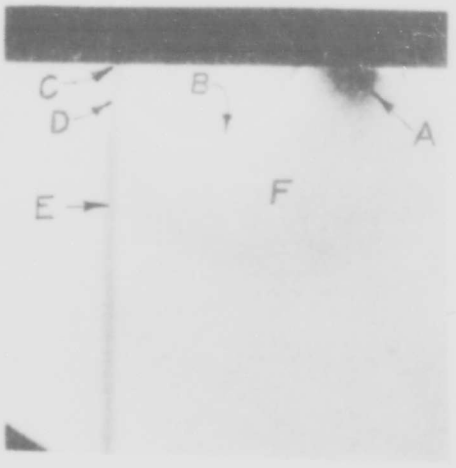

0.750 In. Slot- 1/8 In. Radius

Figure 22. Schlieren Pictures of a Shock Wave Passing Over Various Slot Openings

Continued:

0.400 In. Slot- 1/8 In. Radius

5-0.500 In. Diameter Holes- 1/8 In. Radius

Figure 22 Continued. Schlieren Pictures of a Shock Wave Passing Over Various Slot Openings

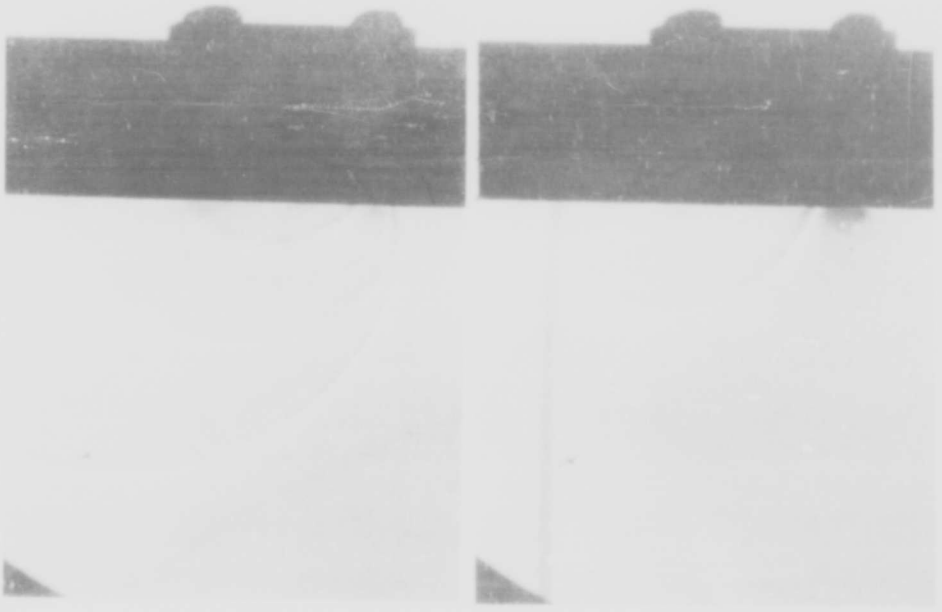

Figure 23. Schlieren Picture of Shock Wave Passing a 0.400 Inch Slot- 3/8 Inch Radius With Plate Over Slot Opening

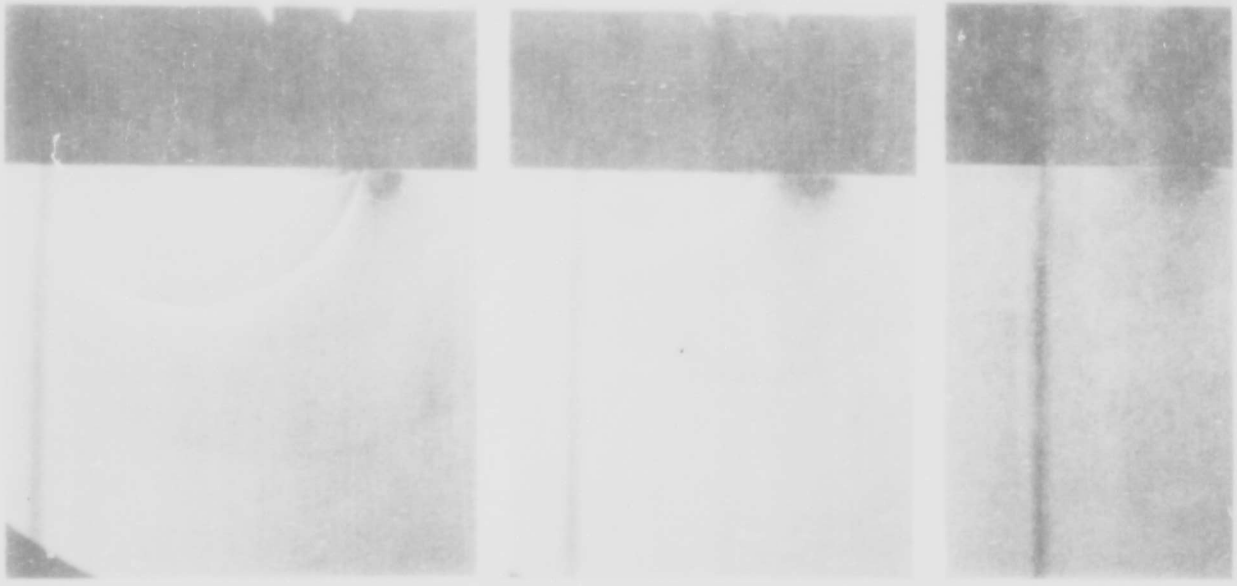

Figure 24. Composite Schlieren Photographs of a Shock Wave Passing a 0.400 Inch Slot- 3/8 Inch Radius

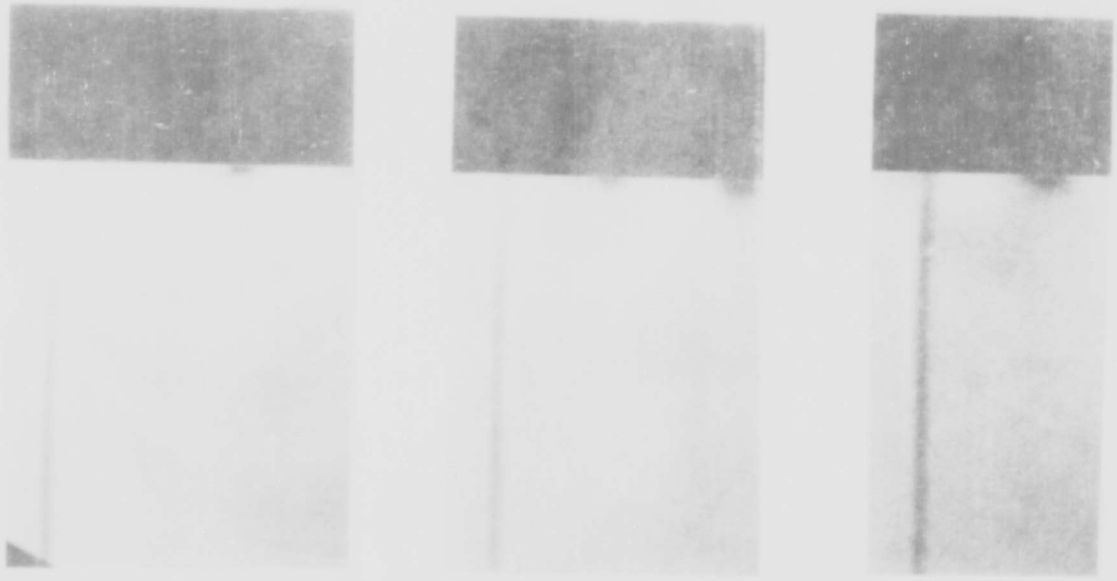

Figure 25. Composite Schlieren Photographs of a Shock Wave Passing Over 5- 0.500 Inch Diameter Holes With 1/4 Inch Entrance Radii

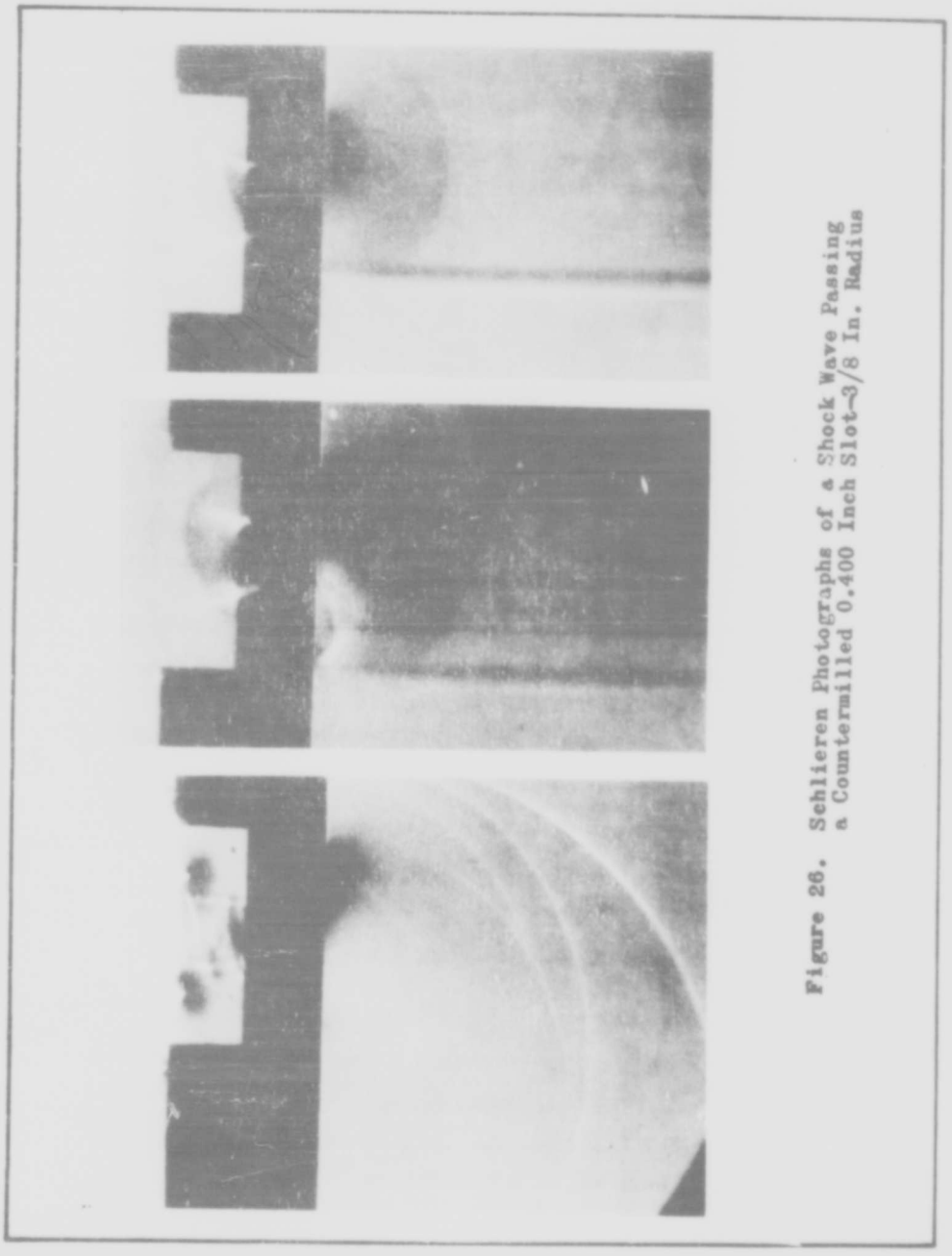

Figure 26. Schlieren Photographs of a Shock Wave Passing a Countermilled 0.400 Inch Slot-3/8 In. Radius

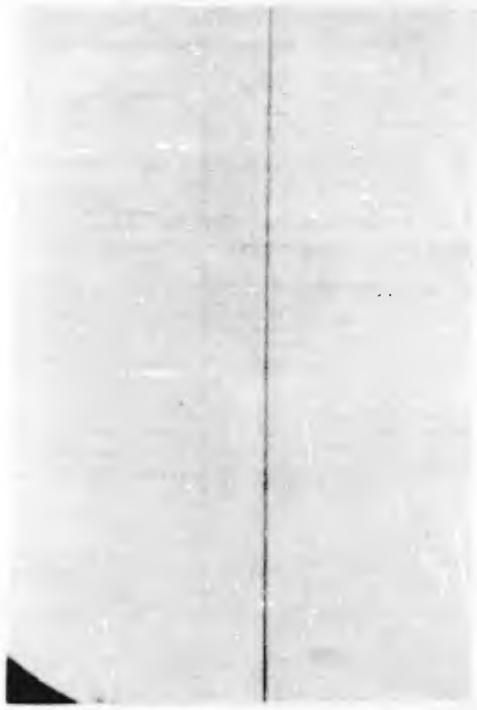

Figure 27. Schlieren Photograph of a Shock Wave in a Test Section Located 7 7/8 Inches Upstream of Station E

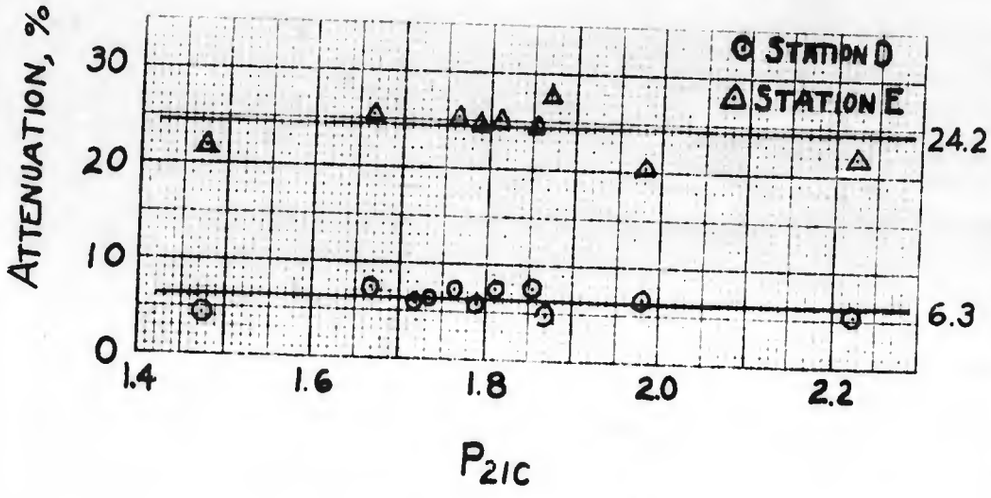

Figure 28. Attenuation at Stations D and E Due to 0.281 Inch Slot With Zero Radius of Entrance

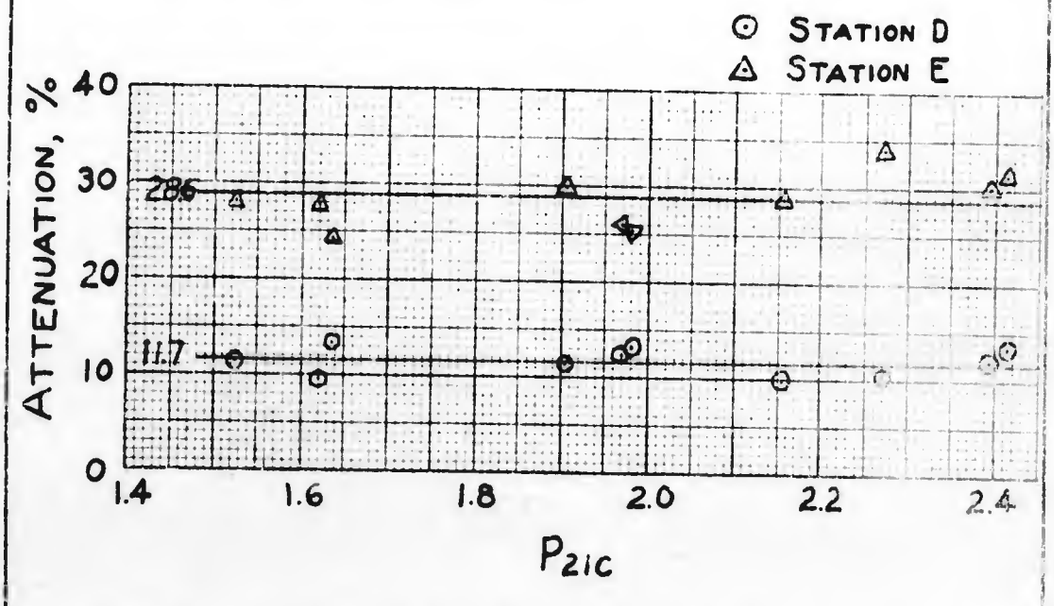

Figure 29. Attenuation at Stations D and E Due to 0.281 Inch Slot With Entrance Radius of 1/8 Inch

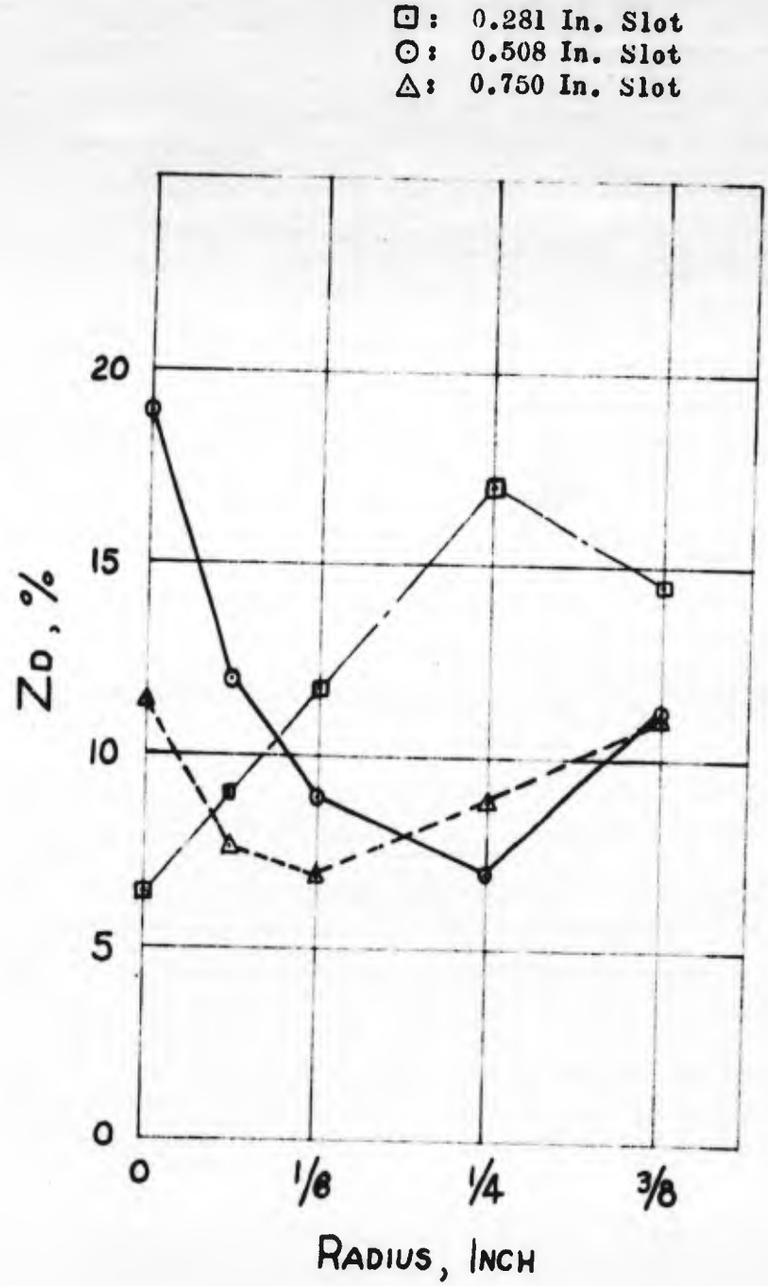

Figure 30. Attenuation at Station D vs. Entrance Radius For Different Slot Openings

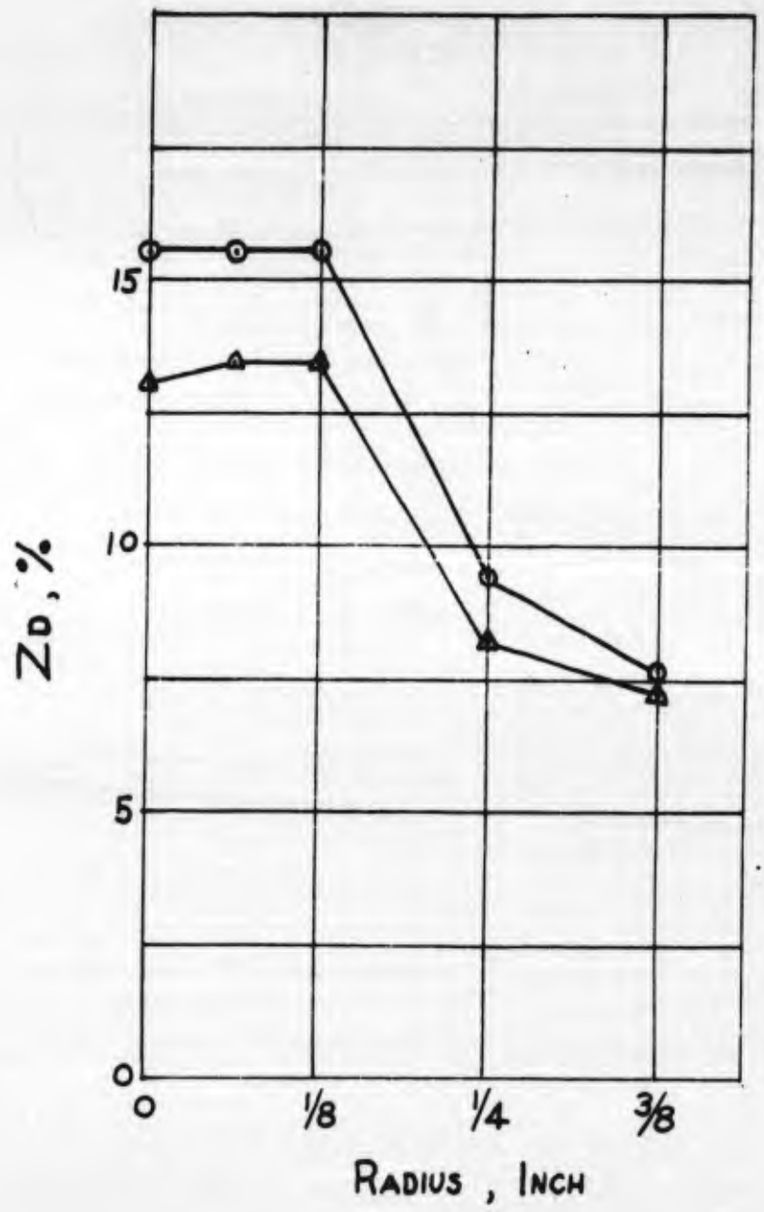

Figure 31. Attenuation at Station D vs. Entrance Radius For 0.400 Inch Slot With and Without 4 Inch Slot Extension

GA/ME/61-5

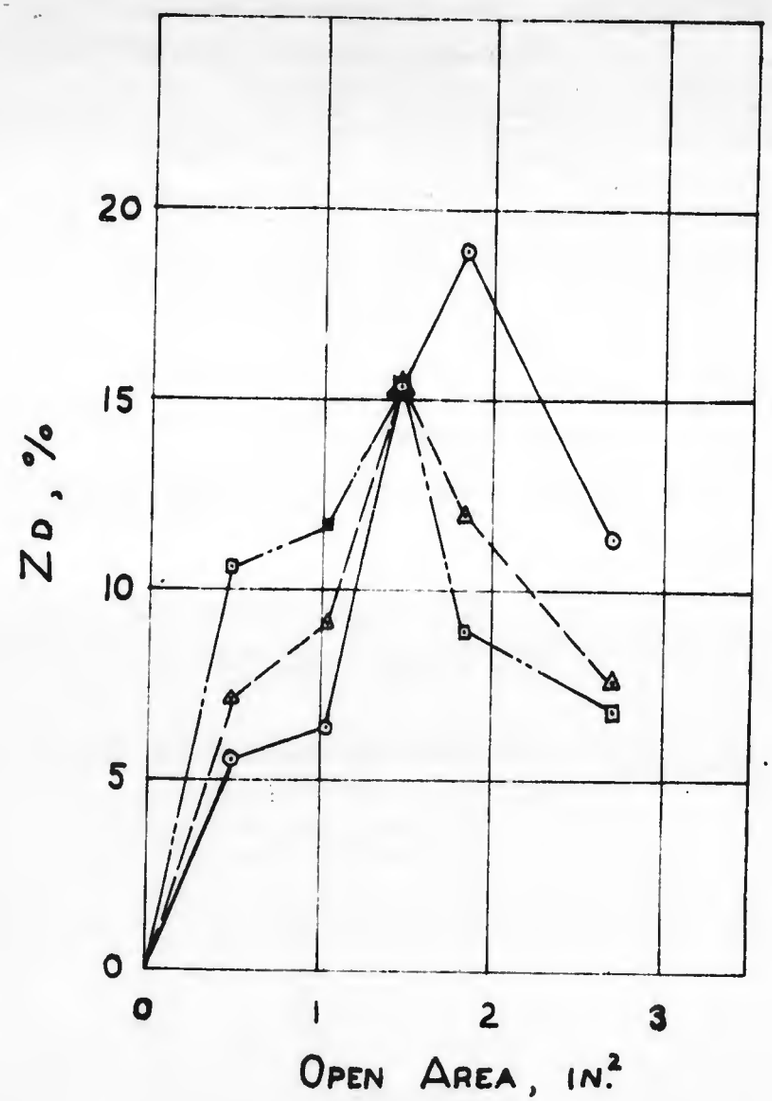

Figure 32. Attenuation at Station D vs. Open Area for Different Entrance Radii

Appendix A

Sample Calibrations For Transducer Calibration Runs

Run #6

Low pressure region initial readings:

$T_1 = 539.5^{\circ}$ R

$p_1 = 14.45$ psia.

Type 531 oscilloscope settings:

Horizontal: 500 microseconds/cm. = 0.0005 sec./cm.

Vertical: 0.20 volts/cm.

Data from oscilloscope photograph:

Horizontal distance from initiation of sweep at station A to the second pressure pulse at station C:

4.35 cm. X 0.0005 sec./cm. = 2.175 millisec.

Vertical deflection @ station B (Transducer #15):

2.80 cm. X 0.20 volts/cm. = 0.560 volts

Vertical deflection @ station C (Transducer #18):

2.70 cm. X 0.20 volts/cm. = 0.540 volts

Shock tube distance between stations A and C = 40in. = 3.33 ft.

Now: $Ws = \frac{\text{distance}}{\text{time}} = \frac{3.33 \text{ ft.}}{2.175 \text{ millisec.}} = 1530$ ft./sec.

Speed of sound in region 1:

For air: $C_1 = 49.1(T_1)^{\frac{1}{2}}$

$C_1 = 49.1(539.5)^{\frac{1}{2}} = 1140$ ft./sec.

Mach number of shock wave = Ms:

$Ms = \frac{Ws}{C_1} = \frac{1530}{1140} = 1.342$

Using equation (2) to find pressure step:

$P_{21} = \frac{7Ms^2-1}{6} = \frac{7(1.342)^2-1}{6} = 1.94$

$p_2 = P_{21} \times p_1 = 1.94 \times 14.45 = 28.00$ psia.

$p_2 - p_1 = 28.00 - 14.45 = 13.55$ psia.

Voltage for this pressure for transducers #15 and #18 is 0.560 volts and 0.540 volts respectively.

Appendix B

Sample Caculations For Z_D of Experimental Run

Run #39

Low pressure region initial readings:

$T_1 = 541.5^{\circ}$ R

$P_1 = 14.30$ psia.

Using Type 531 oscilloscope photograph and Figures 19 and 20:

$(p_2-p_1)_C = 14.23$ psi.

$(p_2-p_1)_D = 13.65$ psi.

Pressure difference in region 2 for stations C and D:

$$p_{2C}-p_{2D} = (p_2-p_1)_C - (p_2-p_1)_D = 14.23 - 13.65 = 0.58$$

Attenuation at station D (Z_D):

From equation (3),

$$Z = \frac{\Delta\frac{p_2}{p_1}}{\frac{p_2}{p_1} - 1} \times 100$$

Therefore, $Z = \frac{\Delta p_2}{(p_2-p_1)_C} \times 100 = \frac{p_{2C}-p_{2D}}{(p_2-p_1)_C} \times 100$

Now, $Z_D = \frac{0.58}{14.23} \times 100 = +4.1\%$

Appendix B

Sample Caculations For Z_D of Experimental Run

Run #39

Low pressure region initial readings:

$T_1 = 541.5^{\circ}$ R

$P_1 = 14.30$ psia.

Using Type 531 oscilloscope photograph and Figures 19 and 20:

$(p_2-p_1)_C = 14.23$ psi.

$(p_2-p_1)_D = 13.65$ psi.

Pressure difference in region 2 for stations C and D:

$$p_{2C}-p_{2D} = (p_2-p_1)_C - (p_2-p_1)_D = 14.23 - 13.65 = 0.58$$

Attenuation at station D (Z_D):

From equation (3),

$$Z = \frac{\Delta\frac{p_2}{p_1}}{\frac{p_2}{p_1} - 1} \times 100$$

Therefore, $Z = \frac{\Delta p_2}{(p_2-p_1)_C} \times 100 = \frac{p_{2C}-p_{2D}}{(p_2-p_1)_C} \times 100$

Now, $Z_D = \frac{0.58}{14.23} \times 100 = +4.1\%$

Appendix C

Analysis of Data Run Scatter

Average Z_D from Table VII for 0.400 inch slot with 1/16 inch radius and no slot extension equals 15.4%. The individual values for Z_D vary from 13.7 to 16.7%.

Though the individual pressure steps, (p_2-p_1), for each station were measured well within the 2% vertical deflection accuracy (0.06 cm. for the 3 centimeter deflection of the average P_{21C} equal to 1.95), a conservative estimate of the measurement errors is 0.02 cm. for station C and 0.04 cm. for station D. Run 142 data with Z_D = 15.6%, close to the average of 15.4%, will be used to illustrate the maximum probable fluctuation in data.

Determine (p_2-p_1) at stations C and D:

$(p_2-p_1)_C$: high value = 13.82 psi.
low value = 13.65 psi.

$(p_2-p_1)_D$: high value = 11.80 psi.
low value = 11.40 psi.

Therefore: $(p_{2C}-p_{2D})_{max.} = 13.82 - 11.40 = 2.42$ psi.

$(p_{2C}-p_{2D})_{min.} = 13.65 - 11.80 = 1.85$ psi.

Now: $Z_{D\ max.} = \frac{2.42}{13.82} \times 100 = 17.5\%$

$Z_{D\ min.} = \frac{1.85}{13.65} \times 100 = 13.5\%$

These values for maximum and minimum attenuation at station D include all values for runs 137 through 144. The values determined are considered very conservative since there are many other factors which could cause scatter of the individual runs for a given configuration.

Vita

Oscar Mauterer was born on [redacted], to [redacted] and [redacted]. He entered the United States Army Air Corps aviation cadet program in September 1943. After graduation from the navigator training phase he served overseas as a B 29 crew member. He was honorably discharged in 1946 and entered Newark College of Engineering where he obtained a degree of Bachelor of Science in Mechanical Engineering in June 1950. He entered the United States Air Force in November 1950 and graduated from the pilot training program. His principal duty assignments have been as a pilot, flight commander, and executive officer in air defense squadrons. Prior to entering the Institute of Technology, he was assigned to the Wright Air Development Center in the Nuclear Weapons Effect Unit of the Aircraft Laboratory.

Permanent address: [redacted]

This thesis was typed by Patricia C. Strick

UNCLASSIFIED